Scaled metal forming experiments: A transport equation approach

DAVEY, K, DARVIZEH, Rooholamin and AL-TAMIMI, A

SCALED METAL FORMING EXPERIMENTS: A TRANSPORT EQUATION APPROACH

K. Davey[*(a,b)], R. Darvizeh[a], A. Al-Tamimi[a]
[a]School of Mechanical, Aerospace and Civil Engineering, The University of Manchester.
[b]The Advanced Forming Research Centre, The University of Strathclyde.

ABSTRACT

The focus of this paper is on a method for the design of bespoke small-scale pilot, metal-forming processes and models that accurately represent corresponding industrial-scale processes. Introducing new complex metal forming processes in industry commonly involves a trial and error approach to ensure that the final product requirements are met. Detailed process modelling, analysis and small-scale feasibility trials could be carried out instead. A fundamental concern of scaled experiments, however, is whether the results obtained can be guaranteed to be representative of the associated industrial processes. Presently, this is not the case with classical approaches founded on dimensional analysis providing little direction for the design of scaled metal-forming experiments. The difficulty is that classical approaches often focus predominantly on constitutive equations (which indirectly represent micro-structural behaviour) and thus focus on aspects that invariably cannot be scaled. This paper introduces a new approach founded on scaled transport equations that describe the physics involved on a finite domain. The transport approach however focuses on physical quantities that do scale and thus provides a platform on which bulk behaviour is accurately represented across the length scales. The new approach is trialled and compared against numerically obtained results to reveal a new powerful technique for scaled experimentation.

Keywords: metal forming; upsetting; transport equations; numerical models; similitude.

[*]keith.davey@manchester.ac.uk

1. INTRODUCTION

Scaled experiments are not new and have found particular traction in fluid-dynamic applications, where models, similarity, dimensional and numerical analysis play an important role [1, 2]. A key theorem underpinning modern dimensional analysis is the Buckingham Pi theorem [3]. If the dimensionless quantities coincide for the full-scale and scaled forming processes, then the two processes are denoted similar. Similar processes will produce corresponding physics but in reality the scaling of complex processes is not so easy and it is seldom possible to match exactly the dimensionless quantities. Similarity can be categorised in three parts: geometric similarity; kinematic similarity and; kinetic similarity [4, 5]. Scaling proportionally is seldom a major difficulty but clearly a requirement of geometric similarity. Kinematic similarity in bulk deformation is concerned with velocities but because geometric similarity is about length scales it is evident that in this context kinematic similarity is about time. Typically, for bulk deformation, kinematic similarity can be achieved by adjustment of the time-scales of the experimental setup. A fundamental difficulty stems from kinetic similarity which is about force proportionality (or drivers more generically), which in general can only be achieved exactly for truly similar systems.

One of the issues with dimensional analysis is that is does not naturally align itself with modern simulation approaches [6]. It is in some sense detached, where the procedure for forming dimensionless quantities is performed in isolation from the procedure involved in direct analysis. A related approach however is the direct rescaling of the governing partial differential equations (should these exist). These equations can be transformed into non-dimensional forms where key non-dimensional quantities will naturally appear as coefficients in these equations. This transformation lends itself to singular-perturbation type analysis approaches if small dimensionless quantities arise in the transformed equations. The approach offers no substantive benefits to numerical analysis although does provide information on the functional relationship between non-dimensional quantities, which is absent from any direct dimensional analysis.

Dimensional analysis has an important part to play in scaled experiments but has limitations [7]. These limitations are particularly pronounced for metal forming processes, where a review of the literature reveals a dearth of serious significant technical works on the subject. Although numerous text books on dimensional analysis exist, few cover solid mechanics [3, 8] and fewer still cover forming (none in fact found). The number of articles involving both dimensional analysis and forming [9, 10] is very limited. Similarity solutions simply do not exist in complex metal forming processes and hence a fundamental difficulty exists when designing scaled experiments.

Transport equations provide a description for the transport of mass, momentum (angular momentum if needed), energy and entropy (displacement has been recently added to this list [11]). The physics of the full-scale industrial process is described by these equations and so is the physics of any scaled model. However, and also, it is possible using Nanson's identities [12] and time rescaling to represent the physics of the full-scale process at the smaller scale and conversely the physics of the smaller scale model at the larger scale. These relationships provide important information. Moving from full scale to the smaller scale provides information on what the model should be, to identically (at least down to the smallest control volume used) represent the physics at the larger scale. Similarly, moving from the small scale to the large scale relays information about what the physics at the small scale is providing at full scale. The reality of the metal forming process is that the scaled processes are not similar but through careful simulation, material selection and choice of lubricant (friction is a major concern in metal forming) a good selection of scaled model can be designed. Up to four simulation types can be identified although any starting geometry and mesh will be identical

for all simulations. The assumption here is that geometric similarity is invoked whilst recognising that numerical codes (finite element (FE) is applied here) have no concept of scale until material properties are input. The four simulation types are:

(i) Full-scale FE simulation of the industrial metal forming process.
(ii) FE simulation of the representation of the full-scale model at the smaller scale.
(iii) FE simulation of the experimental small-scale metal forming process.
(iv) FE simulation of the representation of the small scale model at the larger scale.

The choice of the material, time scale, lubrication, etc. used in the small-scale experiments is informed by the analysis performed in (ii). The analysis in (iii) can be fully supported by experimental trials to refute, support or improve the mathematical models involved or at the very least provide understanding on the limitations of said models. A process of careful technical scrutiny is required at this stage, which could in the worst scenario involve repeated analysis and experimentation. Analysis (iv) provides information on the limitations of said results as seen at the full scale. In practice, some if not all the analyses will likely be performed a number of times prior, during and after any experimental work as the analysis process is most certainly iterative. It is recognised however that his can be problematic for industrially complex flow forming processes providing a practical limit on the number of analyses that can reasonably be performed. It transpires (and confirmed in the paper) that FE analysis is only required for (i) and (iii), with (ii) and (iv) being projections of these analyses, respectively.
In order to explain the concepts involved the paper begins by introducing the mapping underpinning the control volume movements in Section 2 along with possible maps for connecting motion in physical and trial spaces. The transport equations for these spaces are introduced in Section 3 along with a representation of behaviour in the physical space on the trial space. This section focuses on a generic transport equation and establishes the relationships needed for similarity down to the smallest domain considered; this concept is termed *finite similitude*. Section 4 examines the five transport equations of interest to metal forming, i.e. the transport of mass, momentum, movement, energy and entropy. This is followed by an examination of each transport phenomenon in turn, where relationships necessary for the existence of finite similitude are established. The ability to project similar solutions between the trial and physical space and vice versa is considered in Section 6. The importance of this aspect is not fully appreciated in the current literature, yet it provides a mechanism for the design of a physical experiment and the assessment of its representation of the corresponding practical industrial process. An alternative route to scaling is examined in Section 7 where material spaces are utilised. This approach is slightly more involved but is shown to yield the same outcome as the direct mapping approach. Although not too unexpected, the section does address the importance of placing the correct interpretation on the physics as expressed in the material space. The scaling theory presented in the paper being founded on a control volume concept makes no reference to constitutive laws. However, for practical calculations, constitutive behaviour needs to be understood; an aspect covered in Section 8 applied to classical laws. Section 9 looks at the practical limitations of the similarity approach arising from the numbers of independent scaling factors involved. Numerical results are presented in Section 9 to present solutions in both trial and physical spaces for a thermal and relatively simple thermo-mechanical metal forming operations.

2. MAPPINGS FOR SCALING

The mapping theory underpinning the application of scaled transport equations is presented here. The starting point is Euler continuum transport forms applied to a moving control volume Ω_{ps} over the physical space. As depicted in Figure 1 the movement of Ω_{ps} is described by a diffeomorphism $\boldsymbol{x}^*\left(\boldsymbol{X}^*,t\right):\Omega^*_{PS}\mapsto\Omega_{ps}$ where Ω^*_{PS} is a reference space for the control volume. The map can be differentiated with respect to time, whilst holding $\boldsymbol{X}^*$ constant, to obtain the control volume velocity $\underline{v}^*_{ps}=D^*\boldsymbol{x}^*/D^*t$, where $D^*/D^*t=\partial/\partial t\big|_{\boldsymbol{X}^*}$. This formulisation is identical to that employed to derive the material derivative, i.e. $D/Dt=\partial/\partial t\big|_{\boldsymbol{X}}$ and material velocity $\underline{v}=D\boldsymbol{x}^m/Dt$, where $\boldsymbol{x}^m\left(\boldsymbol{X},t\right)$ is a map from a material reference system to the spatial system as depicted in Figure 1. The derivative D^*/D^*t is not common to the literature but plays a crucial role in formularising a rigorous foundation for transport theory along with their correct application to discontinuous physics [13]. The velocity relationship $\underline{v}^*_{ps}=D^*\boldsymbol{x}/D^*t$ can itself be used to define the map $\boldsymbol{x}^*\left(\boldsymbol{X}^*,t\right)$ as it provides a first-order differential equation whose unique solution is guaranteed by Frobenius's theorem [14], which relies on $\underline{v}^*_{ps}$ being sufficiently smooth and on the specification of appropriate initial conditions.

The same apparatus can be invoked to apply to the scaled-trial space in which experimentation is to be performed. In this case, the reference domain Ω^*_{TS} is mapped to the trial space Ω_{ts} with a diffeomorphism $\boldsymbol{s}^*\left(\boldsymbol{S}^*,\tau\right):\Omega^*_{TS}\mapsto\Omega_{ts}$, where allowance is made for the fact that time in the trial space can run at a different rate by use of the symbol τ as opposed to t. Apart possibly from the material map, all the maps discussed thus far are all considered to be diffeomorphisms (i.e. differentiable bijections) and have the role of defining control volume movement. The velocity $\underline{v}^*_{ts}$ of Ω_{ts} is described using the star derivative $D^*/D^*\tau\equiv\partial/\partial\tau\big|_{\boldsymbol{s}^*}$, i.e. $\underline{v}^*_{ts}=D^*\boldsymbol{s}^*/D^*\tau$. With the maps defined the following differentials exist:

$$dx^*_i=\frac{\partial x^*_i}{\partial X^*_j}dX^*_j+\left.\frac{\partial x^*_i}{\partial t}\right|_{\boldsymbol{X}^*}dt \tag{1}$$

and

$$ds^*_i=\frac{\partial s^*_i}{\partial S^*_j}dS^*_j+\left.\frac{\partial s^*_i}{\partial \tau}\right|_{\boldsymbol{s}^*}d\tau \tag{2}$$

succinctly written as $\boldsymbol{dx}^*=F^{x^*}_{X^*}\otimes\boldsymbol{dX}^*+\underline{v}^*_{ps}dt$ and $\boldsymbol{ds}^*=F^{s^*}_{S^*}\otimes\boldsymbol{dS}^*+\underline{v}^*_{ts}d\tau$, respectively, and where the control volume deformation gradient tensors are $F^{x^*}_{X^*}=\partial\boldsymbol{x}^*/\partial\boldsymbol{X}^*$ and $F^{s^*}_{S^*}=\partial\boldsymbol{s}^*/\partial\boldsymbol{S}^*$. Similarly, a material point $\boldsymbol{S}$ in Ω_{TS} is mapped to Ω^m_{ts} via the assumed diffeomorphism $\boldsymbol{s}^m\left(\boldsymbol{S},\tau\right):\Omega_{TS}\mapsto\Omega^m_{ts}$, where Ω_{TS} is a material reference space and Ω^m_{ts} is a region in the physical space. Likewise, a material point $\boldsymbol{X}$ in Ω_{PS} is mapped to Ω^m_{ps} via the diffeomorphism $\boldsymbol{x}^m\left(\boldsymbol{X},\tau\right):\Omega_{PS}\mapsto\Omega^m_{ps}$, where Ω_{PS} the material reference space for Ω^m_{ps} (see Figure 1).

There exists also a map to encapsulate the scaling between the trial and physical spaces. This can manifest itself in one of two ways, i.e. by a direct map between Ω_{ts} and Ω_{ps} or indirectly via a map between Ω_{TS} and Ω_{PS} (or more correctly Ω^*_{TS} and Ω^*_{PS}). The former map is a less convoluted approach and at its most simplest is represented by the mathematical relationship $\boldsymbol{dx}^* = F_{s^*}^{x^*} \otimes \boldsymbol{ds}^*$, where for scaling factor β and isotropic scaling, $F_{s^*}^{x^*} = \beta I$, with identity tensor I. In addition, the time scales in the trial and physical space are related by $dt = h(\tau)d\tau$ or $d\tau = g(t)dt$, where $h(\tau)g(t) = 1$, where h and g are bijection maps. It is important to appreciate here that the relationship $\boldsymbol{dx}^* = F_{s^*}^{x^*} \otimes \boldsymbol{ds}^*$ (being an exact differential) immediately infers that $\boldsymbol{x}^*$ is solely a function of $\boldsymbol{s}^*$. Similarly, the material-space route invokes identical time scaling but utilises $\boldsymbol{dX}^* = F_{S^*}^{X^*} \otimes \boldsymbol{dS}^*$, where $F_{S^*}^{X^*} = \beta I$ and control volumes Ω^*_{TS} and Ω^*_{PS} are contained in the respective material spaces. The movement of control volumes over a material space requires particular care, so initial consideration is given to scaled transport equations on the physical spaces.

3. TRANSPORT THEORY ON PHYSICAL SPACES

A general conservation law in transport form for some physical quantity ψ governing the physics on a moving control volume Ω_{ps} is

$$\frac{D^*}{D^*t}\int_{\Omega_{ps}} \rho_{ps}\psi_{ps}\,dV_{ps} + \int_{\Gamma_{ps}} \rho_{ps}\psi_{ps}\left(\underline{v}_{ps} - \underline{v}^*_{ps}\right)\cdot\underline{n}_{ps}\,d\Gamma_{ps} = -\int_{\Gamma_{ps}} \underline{J}^{\psi}_{ps}\cdot\underline{n}_{ps}\,d\Gamma_{ps} + \int_{\Omega_{ps}} \rho_{ps}b^{\psi}_{ps}\,dV_{ps} \qquad (3)$$

where ρ is density, $\underline{v}$ is material velocity, $\underline{J}\cdot\underline{n}$ is a flux, b is a source term [15] and Γ is the boundary for Ω.

Note the use of D^*/D^*t rather than the ordinary derivative d/dt in Equation (3) even though these are identical when applied to a function of t. The use of the derivative D^*/D^*t in (3) is intended to immediately relay the notion that Ω_{ps} is a control volume transported by means of the velocity $\underline{v}^*_{ps}$. Consider further an equivalent transport equation for the trial space control volume Ω_{ts} transported with velocity $\underline{v}^*_{ts}$, i.e.

$$\frac{D^*}{D^*\tau}\int_{\Omega_{ts}} \rho_{ts}\psi_{ts}\,dV_{ts} + \int_{\Gamma_{ts}} \rho_{ts}\psi_{ts}\left(\underline{v}_{ts} - \underline{v}^*_{ts}\right)\cdot\underline{n}_{ts}\,d\Gamma_{ts} = -\int_{\Gamma_{ts}} \underline{J}^{\psi}_{ts}\cdot\underline{n}_{ts}\,d\Gamma_{ts} + \int_{\Omega_{ts}} \rho_{ts}b^{\psi}_{ts}\,dV_{ts} \qquad (4)$$

Equation (3) and (4) are currently unrelated and describe the transport phenomena in their respective spaces. However, Equation (3) can be transformed into a form that appears rather similar to Equation (4). This can be achieved by assuming the existence of the direct map $\boldsymbol{x}^*(\boldsymbol{s}^*, \tau)$, whose differential is

$$dx^*_i = \frac{\partial x^*_i}{\partial s^*_j}ds^*_j + \left.\frac{\partial x^*_i}{\partial \tau}\right|_{\mathbf{s}} d\tau \qquad (5)$$

succinctly written as $\boldsymbol{dx}^* = F_{s^*}^{x^*} \otimes \boldsymbol{ds}^* + \underline{v}^{rel} d\tau$ and given that $d\tau = g(t)dt$ is also equal to $\boldsymbol{dx}^* = F_{s^*}^{x^*} \otimes \boldsymbol{ds}^* + g\underline{v}^{rel} dt$ although as mentioned above reduces further to $\boldsymbol{dx}^* = F_{s^*}^{x^*} \otimes \boldsymbol{ds}^*$ with $\boldsymbol{x}^*$ assumed a function of $\boldsymbol{s}^*$ only.

Equation (5) gives rise to Nanson's geometric identities $dV_{ps} = \left|F_{s^*}^{x^*}\right| dV_{ts}$ and $\mathbf{d\Gamma}_{ps} = \left|F_{s^*}^{x^*}\right| \mathbf{d\Gamma}_{ts} \otimes \left(F_{s^*}^{x^*}\right)^{-1}$, where $\mathbf{d\Gamma}_{ps} = \underline{n}_{ps} \mathrm{d}\Gamma_{ps}$ and $\mathbf{d\Gamma}_{ts} = \underline{n}_{ts} \mathrm{d}\Gamma_{ts}$ [12] . Substitution of these into Equation (3) gives

$$\frac{1}{h(\tau)} \frac{D^*}{D^*\tau} \int_{\Omega_{ts}^*} \rho_{ps}\psi_{ps} \left|F_{s^*}^{x^*}\right| dV_{ts} + \int_{\Gamma_{ts}^*} \rho_{ps}\psi_{ps} \left|F_{s^*}^{x^*}\right| \left(F_{s^*}^{x^*}\right)^{-1} \otimes \left(\underline{v}_{ps} - \underline{v}_{ps}^*\right) \cdot \underline{n}_{ts} d\Gamma_{ts} =$$

$$- \int_{\Gamma_{ts}^*} \left|F_{s^*}^{x^*}\right| \left(F_{s^*}^{x^*}\right)^{-1} \otimes \underline{J}_{ps}^{\psi} \cdot \underline{n}_{ts} d\Gamma_{ts} + \int_{\Omega_{ts}^*} \rho_{ps} b_{ps}^{\psi} \left|F_{s^*}^{x^*}\right| dV_{ts} \qquad (6)$$

where $dt = h(\tau)d\tau$ relays the relationship between time in the trial and physical space.

It should be appreciated that an implicit assumption invoked here is that the control volumes in Equations (6) and (4) are identical. There is however, an element of choice when it comes to control-volume selection for any analysis making such an assumption appear not unreasonable. The control volume applicable to Equation (6) however is dictated by the map $\boldsymbol{x}^*(\boldsymbol{s}^*, \tau) : \Omega_{ts} \mapsto \Omega_{ps}$. This is not the case for Equation (4) where an element of choice is possible and in this case invoked to provide matching control volumes in the trial space. Equation (6) and (4) are identical if $\rho_{ps}\psi_{ps} \left|F_{s^*}^{x^*}\right| = \rho_{ts}\psi_{ts}$, $h\left(F_{s^*}^{x^*}\right)^{-1} \otimes \left(\underline{v}_{ps} - \underline{v}_{ps}^*\right) = \underline{v}_{ts} - \underline{v}_{ts}^*$, $h\left|F_{s^*}^{x^*}\right| \left(F_{s^*}^{x^*}\right)^{-1} \otimes \underline{J}_{ps}^{\psi} = \underline{J}_{ts}^{\psi}$ and $h\rho_{ps} b_{ps}^{\psi} \left|F_{s^*}^{x^*}\right| = \rho_{ts} b_{ts}^{\psi}$. Note however that slightly greater generality can be acquired if Equation (6) is multiplied by a scalar α^{ψ} (along with h) and on matching again gives

$$\rho_{ts}\psi_{ts} = \alpha^{\psi} \rho_{ps}\psi_{ps} \left|F_{s^*}^{x^*}\right| \qquad (7a)$$

$$\underline{v}_{ts} - \underline{v}_{ts}^* = h\left(F_{s^*}^{x^*}\right)^{-1} \otimes \left(\underline{v}_{ps} - \underline{v}_{ps}^*\right) \qquad (7b)$$

$$\underline{J}_{ts}^{\psi} = \alpha^{\psi} h \left|F_{s^*}^{x^*}\right| F_s^{-1} \cdot \underline{J}_{ps}^{\psi} \qquad (7c)$$

and

$$\rho_{ts}^{\psi} b_{ts} = \alpha^{\psi} h \rho_{ps} b_{ps}^{\psi} \left|F_{s^*}^{x^*}\right| \qquad (7d)$$

where setting $\underline{v}_{ts}^* = h\left(F_{s^*}^{x^*}\right)^{-1} \otimes \underline{v}_{ps}^*$ and $\underline{v}_{ts} = h\left(F_{s^*}^{x^*}\right)^{-1} \otimes \underline{v}_{ps}$ is sufficient for Equation (7b).

The identify $\underline{v}_{ts}^* = h\left(F_{s^*}^{x^*}\right)^{-1} \otimes \underline{v}_{ps}^*$ has little to do with choice however and is a direct

consequence of the relationship between Ω^*_{ts} and Ω^*_{ps}. Substitution of $\boldsymbol{ds}^* = F^{s^*}_{S^*} \otimes \boldsymbol{dS}^* + \underline{v}^*_{ts} d\tau$ into $\boldsymbol{dx}^* = F^{x^*}_{s^*} \otimes \boldsymbol{ds}^* + \underline{v}^{rel} d\tau$ gives

$$\boldsymbol{dx}^* = F^{x^*}_{s^*} F^{s^*}_{S^*} \otimes \boldsymbol{dS}^* + \left(F^{x^*}_{s^*} \otimes \underline{v}^*_{ts} + \underline{v}^{rel} \right) d\tau \tag{8}$$

which can be contrasted with $\boldsymbol{dx}^* = F^{x^*}_{X^*} \otimes \boldsymbol{dX}^* + \underline{v}^*_{ps} dt$, where under the assumption that reference control volumes Ω^*_{TS} and Ω^*_{PS} are temporally invariant, reveals the identity

$$h\underline{v}^*_{ps} = F^{x^*}_{s^*} \otimes \underline{v}^*_{ts} + \underline{v}^{rel} \tag{9}$$

which reduces to $\underline{v}^*_{ts} = h\left(F^{x^*}_{s^*} \right)^{-1} \otimes \underline{v}^*_{ps}$ for $\underline{v}^{rel} = \underline{0}$.

The condition $\underline{v}^{rel} = \underline{0}$ applies for the situation where the movement of the two control volumes Ω^*_{ts} and Ω^*_{ps} are synchronised, which is a reasonable requirement for any matched analysis.

4. THE EXISTENCE OF SIMILAR EQUATIONS

Equation (7) provides the identities sufficient for isotropic scaling that are required to be satisfied for a similar system. For the isotropic scaling with constant scaling factor β the control volume deformation gradient tensor $F^{x^*}_{s^*} = \beta I$. It follows that $\left| F^{x^*}_{s^*} \right| = \beta^3$ (in 3D) and Equation (7) reduces to

$$\rho_{ts} \psi_{ts} = \alpha^{\psi} \beta^3 \rho_{ps} \psi_{ps} \tag{10a}$$

$$\underline{v}^*_{ts} = h\beta^{-1} \underline{v}^*_{ps} \tag{10b}$$

$$\underline{v}_{ts} = h\beta^{-1} \underline{v}_{ps} \tag{10c}$$

$$\underline{J}^{\psi}_{ts} = \alpha^{\psi} h\beta^2 \underline{J}^{\psi}_{ps} \tag{10d}$$

and

$$\rho_{ts} b^{\psi}_{ts} = \alpha^{\psi} h\beta^3 \rho_{ps} b^{\psi}_{ps} \tag{10e}$$

where (10c) provides kinematic similarity, and where kinetic similarity principally arises from (10d) and to a lesser extent (10e).

For a particular transport equation that there is a good possibility of being able to select a set ρ_{ts}, ψ_{ts}, $\underline{v}^*_{ts}$, $\underline{v}_{ts}$, $\underline{J}^{\psi}_{ts}$ and b^{ψ}_{ts} along with h and α^{ψ} to enable Equation (6) and (4) to match. The challenge however is to match all those transport equations of interest to metal forming, which can only happen for truly similar systems. The transport equations of interest in metal

forming are equations for continuity, momentum, displacement, energy and entropy, which are

$$\frac{D^*}{D^*t}\int_{\Omega_{ps}} \rho_{ps} dV + \int_{\Gamma_{ps}} \rho_{ps}\left(\underline{v}_{ps} - \underline{v}^*_{ps}\right)\cdot \underline{n}_{ps} d\Gamma_{ps} = 0 \tag{11}$$

$$\frac{D^*}{D^*t}\int_{\Omega_{ps}} \rho_{ps}\underline{v}_{ps} dV + \int_{\Gamma_{ps}} \rho_{ps}\underline{v}_{ps}\left(\underline{v}_{ps} - \underline{v}^*_{ps}\right)\cdot \underline{n}_{ps} d\Gamma = \int_{\Gamma_{ps}} \underline{\underline{\sigma}}_{ps}\cdot \underline{n}_{ps} d\Gamma_{ps} + \int_{\Omega} \rho_{ps}\underline{b}_{ps} dV_{ps} \tag{12}$$

$$\frac{D^*}{D^*t}\int_{\Omega_{ps}} \rho_{ps}\underline{u}_{ps} dV_{ps} + \int_{\Gamma} \rho_{ps}\underline{u}_{ps}\left(\underline{v}_{ps} - \underline{v}^*_{ps}\right)\cdot \underline{n}_{ps} d\Gamma_{ps} = \int_{\Omega_{ps}} \rho_{ps}\underline{v}_{ps} dV_{ps} \tag{13}$$

$$\frac{D^*}{D^*t}\int_{\Omega_{ps}} \rho_{ps} e_{ps} dV_{ps} + \int_{\Gamma_{ps}} \rho_{ps} e_{ps}\left(\underline{v}_{ps} - \underline{v}^*_{ps}\right)\cdot \underline{n}_{ps} d\Gamma_{ps} =$$
$$\int_{\Gamma_{ps}} \underline{v}_{ps}\cdot\underline{\underline{\sigma}}_{ps}\cdot \underline{n}_{ps} d\Gamma_{ps} - \int_{\Gamma_{ps}} \underline{q}_{ps}\cdot \underline{n}_{ps} d\Gamma_{ps} + \int_{\Omega_{ps}} \rho_{ps} Q_{ps} dV + \int_{\Omega_{ps}} \rho_{ps}\underline{v}_{ps}\cdot\underline{b}_{ps} dV_{ps} \tag{14}$$

$$\frac{D^*}{D^*t}\int_{\Omega_{ps}} \rho_{ps} s_{ps} dV_{ps} + \int_{\Gamma_{ps}} \rho_{ps} s_{ps}\left(\underline{v}_{ps} - \underline{v}^*_{ps}\right)\cdot \underline{n}_{ps} d\Gamma_{ps} =$$
$$-\int_{\Gamma_{ps}} T^{-1}_{ps}\underline{q}_{ps}\cdot \underline{n}_{ps} d\Gamma_{ps} + \int_{\Omega_{ps}} \rho_{ps} T^{-1}_{ps} Q_{ps} dV_{ps} + \dot{S}_i \tag{15}$$

where $e = u + \frac{1}{2}\underline{v}\cdot\underline{v}$, u is stationary internal specific energy, and s is specific entropy, $\underline{q}\cdot\underline{n}$ is heat flux, Q represents a heat source, $\underline{\underline{\sigma}}$ is the Cauchy stress tensor, $\underline{b}$ is a body force and $\dot{S}_i \geq 0$ is associated with irreversibility.

Note that ψ can be identified with unity, velocity, displacement, energy and entropy by setting ψ to be either 1, $\underline{v}$, $\underline{u}$, e, or s in Equations (3) and (4).

5. PRACTICAL SIMULARITY CONDITIONS

It is shown in this section how taking each transport equation in turn starting from continuity and ending with entropy imposes constraints on the parameters and functions in the similarity conditions of Equation (10).

5.1. The problem with mass

Consider then the requirements of continuity (i.e. $\psi_{ts} = \psi_{ps} = 1$) where for a similar system Equation (10) gives $\rho_{ts} = \alpha^\rho \beta^3 \rho_{ps}$, $\underline{v}^*_{ts} = h\beta^{-1}\underline{v}^*_{ps}$, $\underline{v}_{ts} = h\beta^{-1}\underline{v}_{ps}$, $\underline{J}^1_{ts} = \underline{0}$ and $\rho_{ts} b^1_{ts} = 0$. The relationship of principal interest here is

$$\rho_{ts} = \alpha^\rho \beta^3 \rho_{ps} \tag{16}$$

although typically for metal forming density is reasonably invariant. The parameter β is dictated by the scaling involved in the experimental trial so is somewhat constrained. However, the parameter α^ρ can be set to facilitate the selection of an experimental material as regards density. An example might be a steel-lead combination where for instance

$$\alpha^{\rho} = \frac{1}{\beta^3}\frac{\rho_{lead}}{\rho_{steel}} \tag{17}$$

should suffice with prescribed values for ρ_{steel} and ρ_{lead}.

It is clear therefore that density is constrained by the continuity equation by a relationship of the form $\rho_{ts}\rho_{steel} = \rho_{lead}\rho_{ps}$. This relationship is not the only constraint as the identity $\underline{v}_{ts} = h\beta^{-1}\underline{v}_{ps}$ imposes restrictions on the velocity field $\underline{v}_{ts}$, which might be expected to be problematic for momentum. Note also that the relationship $\underline{v}^{*}_{ts} = h\beta^{-1}\underline{v}^{*}_{ps}$ is dictating the response of the control volume Ω^{*}_{ts} given the response of Ω^{*}_{ps}.

5.2. The problem with momentum

For a similar system, continuity restricts density to satisfy $\rho_{ts} = \alpha^{\rho}\beta^3\rho_{ps}$ and it can be anticipated that momentum will provide a similar restriction for $\underline{v}_{ts}$. However, as already alluded to, continuity similarity also required the constraint $\underline{v}_{ts} = h\beta^{-1}\underline{v}_{ps}$. Equation (10) for momentum gives firstly $\rho_{ts}\underline{v}_{ts} = \alpha^{\underline{v}}\beta^3\rho_{ps}\underline{v}_{ps}$, which on assumption that the relationship $\rho_{ts} = \alpha^{\rho}\beta^3\rho_{ps}$ is satisfied, reduces to

$$\alpha^{\rho}\underline{v}_{ts} = \alpha^{\underline{v}}\underline{v}_{ps} \tag{18}$$

This can be contrasted against the relationship $\underline{v}_{ts} = h\beta^{-1}\underline{v}_{ps}$ and immediately infers that the function $h(\tau)$ is a constant (as yet unspecified) and

$$\alpha^{\underline{v}} = h\beta^{-1}\alpha^{\rho} \tag{19}$$

Note also from Equations (10d) and (10e) that $\underline{\underline{\sigma}}_{ts} = \alpha^{\underline{v}}h\beta^2\underline{\underline{\sigma}}_{ps}$ and $\rho_{ts}\underline{b}_{ts} = \alpha^{\underline{v}}h\beta^3\rho_{ps}\underline{b}_{ps}$. With the constitutive response $\underline{\underline{\sigma}}'_{ts} : \underline{\underline{\sigma}}'_{ts} = \frac{2}{3}\bar{\sigma}^2_{ts}$ and $\underline{\underline{\sigma}}'_{ps} : \underline{\underline{\sigma}}'_{ps} = \frac{2}{3}\bar{\sigma}^2_{ps}$, where $\bar{\sigma}$ is an effective stress (current yield stress) and $\underline{\underline{\sigma}}'$ denotes a deviatoric stress tensor, it can be inferred from the identity $\underline{\underline{\sigma}}_{ts} = \alpha^{\underline{v}}h\beta^2\underline{\underline{\sigma}}_{ps}$ that $\underline{\underline{\sigma}}'_{ts} = \alpha^{\underline{v}}h\beta^2\underline{\underline{\sigma}}'_{ps}$. It follows that $\bar{\sigma}_{ts} = \alpha^{\underline{v}}h\beta^2\bar{\sigma}_{ps}$ or $\bar{\sigma}_{ts} = \alpha^{\rho}h^2\beta\bar{\sigma}_{ps}$ or $h^2 = \left(\alpha^{\rho}\beta\right)^{-1}\bar{\sigma}^{-1}_{ps}\bar{\sigma}_{ts}$, which infers that the time-scales in the trial space have to set be cater for the different material yield strengths, i.e.

$$h = \sqrt{\frac{1}{\alpha^{\rho}\beta}\frac{Y_{ts}}{Y_{ps}}} \tag{20}$$

where *Y* refers to yield strength.

This result is not too surprising because the stress relates back to the forces involved and

hence the rate of material movement.

5.3. The problem with movement

Equation (10) for movement provides the similarity condition $\rho_{ts}\underline{u}_{ts} = \alpha^{\underline{u}}\beta^3\rho_{ps}\underline{u}_{ps}$, which in view of the relationship $\rho_{ts} = \alpha^{\rho}\beta^3\rho_{ps}$ reduces to

$$\alpha^{\rho}\underline{u}_{ts} = \alpha^{\underline{u}}\underline{u}_{ps} \tag{21}$$

which at first sight appears unproblematic.

Note also from Equation (10e) that $\rho_{ts}\underline{v}_{ts} = \alpha^{\underline{u}}h\beta^3\rho_{ps}\underline{v}_{ps}$ which on substitution of $\rho_{ts} = \alpha^{\rho}\beta^3\rho_{ps}$ gives $\alpha^{\rho}\underline{v}_{ts} = \alpha^{\underline{u}}h\underline{v}_{ps}$. However, in order to satisfy Equation (18) it is necessary that

$$h\alpha^{\underline{u}} = \alpha^{\underline{v}} = \frac{h}{\beta}\alpha^{\rho} \tag{22}$$

which means that Equation (21) gives $\beta\underline{u}_{ts} = \underline{u}_{ps}$.

There is little choice with movement as no free factors exist, which is no surprise because on differentiation of $\beta\underline{u}_{ts} = \underline{u}_{ps}$ with respect to time must return Equation (18) or equivalently $\beta\underline{v}_{ts} = h\underline{v}_{ps}$. Note that a scaled space infers that a material element in one space can be related to a material element in the other in the manner $\boldsymbol{dx}^m = F_{s^*}^{x^*} \otimes \boldsymbol{ds}^m = \beta\boldsymbol{ds}^m$, which is precisely $\underline{du}_{ps} = \beta\underline{du}_{ts}$. Differentiation with respect to *t* and noting that $dt = hd\tau$, returns the expected and required relationship $\beta\underline{v}_{ts} = h\underline{v}_{ps}$.

5.4. The problem with energy

Following the same approach for energy reveals $\rho_{ts}e_{ts} = \alpha^{e}\beta^3\rho_{ps}e_{ps}$, which reduces to

$$\alpha^{\rho}e_{ts} = \alpha^{e}e_{ps} \tag{23}$$

or more fully

$$\alpha^{\rho}\left(u_{ts} + \tfrac{1}{2}v_{ts}^2\right) = \alpha^{e}\left(u_{ps} + \tfrac{1}{2}v_{ps}^2\right) \tag{24}$$

where $v_{ts}^2 = \underline{v}_{ts}\cdot\underline{v}_{ts}$ and $v_{ps}^2 = \underline{v}_{ps}\cdot\underline{v}_{ps}$ but since Equation (18) is $\alpha^{\rho}\underline{v}_{ts} = \alpha^{\underline{v}}\underline{v}_{ps}$ the scalar identity $\alpha^{\rho}v_{ts} = \alpha^{\underline{v}}v_{ps}$ immediately follows and consequently it is sufficient for α^{e} to satisfy

$$\alpha^{\rho}\alpha^{e} = \left(\alpha^{\underline{v}}\right)^2 \tag{25}$$

and

$$\alpha^{\rho} u_{ts} = \alpha^{e} u_{ps} \tag{26}$$

for Equation (24) to be satisfied.
Note however, that Equation (10d) yields

$$\underline{v}_{ts} \otimes \underline{\underline{\sigma}}_{ts} = \alpha^{e} h \beta^{2} \underline{v}_{ps} \otimes \underline{\underline{\sigma}}_{ps} \tag{27}$$

but $\underline{\underline{\sigma}}_{ts} = \alpha^{v} h \beta^{2} \underline{\underline{\sigma}}_{ps}$ and $\alpha^{\rho} \underline{v}_{ts} = \alpha^{v} \underline{v}_{ps}$, which on performing a tensor product produces $\alpha^{\rho} \underline{v}_{ts} \otimes \underline{\underline{\sigma}}_{ts} = \alpha^{v} \alpha^{v} h \beta^{2} \underline{v}_{ps} \otimes \underline{\underline{\sigma}}_{ps} = \alpha^{\rho} \alpha^{e} h \beta^{2} \underline{v}_{ps} \otimes \underline{\underline{\sigma}}_{ps}$, which confirms the consistency of Equations (18), the stress tensor relationship $\underline{\underline{\sigma}}_{ts} = \alpha^{v} h \beta^{2} \underline{\underline{\sigma}}_{ps}$ and Equation (27).
Note also that Equation (10e), if applied to the mechanical energy source term in Equation (14), gives the relationship

$$\rho_{ts} \underline{v}_{ts} \cdot \underline{b}_{ts} = \alpha^{e} h \beta^{3} \rho_{ps} \underline{v}_{ps} \cdot \underline{b}_{ps} \tag{28}$$

but on substitution of $\beta \underline{v}_{ts} = h \underline{v}_{ps}$ and $\rho_{ts} \underline{b}_{ts} = \alpha^{v} h \beta^{3} \rho_{ps} \underline{b}_{ps}$ into the left had side of this expression returns $\beta \rho_{ts} \underline{v}_{ts} \cdot \underline{b}_{ts} = \alpha^{v} h^{2} \beta^{3} \rho_{ps} \underline{v}_{ps} \cdot \underline{b}_{ps}$.
However, in view of the identity $\alpha^{\rho} \alpha^{e} = \alpha^{v} \alpha^{v}$ this expression reduces to $\beta \alpha^{v} \rho_{ts} \underline{v}_{ts} \cdot \underline{b}_{ts} = \alpha^{\rho} \alpha^{e} h^{2} \beta^{3} \rho_{ps} \underline{v}_{ps} \cdot \underline{b}_{ps}$ and reduces further on substitution of $\alpha^{v} = h \beta^{-1} \alpha^{\rho}$ to $\alpha^{\rho} h \rho_{ts} \underline{v}_{ts} \cdot \underline{b}_{ts} = \alpha^{\rho} \alpha^{e} h^{2} \beta^{3} \rho_{ps} \underline{b}_{ps} \cdot \underline{v}_{ts}$, which on cancellation of $\alpha^{\rho} h$ from both sides confirms the consistency of Equation (28).
Note finally from Equation (10c) applied to the heat-flux term in Equation (14), that

$$\underline{q}_{ts} = \alpha^{e} h \beta^{2} \underline{q}_{ps} \tag{29}$$

5.5. The problem with entropy

The left hand side of entropy Equation (15) provides $\rho_{ts} s_{ts} = \alpha^{s} \beta^{3} \rho_{ps} s_{ps}$, which reduces to

$$\alpha^{\rho} s_{ts} = \alpha^{s} s_{ps} \tag{30}$$

but more constraining is the entropy transfer term which on application of Equation (10d) yields

$$\frac{\underline{q}_{ts}}{T_{ts}} = \alpha^{s} h \beta^{2} \frac{\underline{q}_{ps}}{T_{ps}} \tag{31}$$

but note that Equation (29) is $\underline{q}_{ts} = \alpha^{e} h \beta^{2} \underline{q}_{ps}$, which on substitution reveals

$$\frac{\alpha^{e}}{T_{ts}} = \frac{\alpha^{s}}{T_{ps}} \tag{32}$$

or equivalently $\alpha^s T_{ts} = \alpha^e T_{ps}$ and thus providing a proportional relationship between temperature.

The main function of the scaling parameter α^s is to account for the possibility that temperatures in the physical and trial spaces can be different although proportional for similarity. Observe also the heat-source term in Equation (15) gives $\rho_{ts} Q_{ts} T_{ts}^{-1} = \alpha^s h \beta^3 \rho_{ps} Q_{ps} T_{ps}^{-1}$ but energy returns $\rho_{ts} Q_{ts} = \alpha^e h \beta^3 \rho_{ps} Q_{ps}$, which on substitution returns $\alpha^e T_{ts}^{-1} = \alpha^s T_{ps}^{-1}$, which is just Equation (32), so consistent behaviour is returned.

An interesting aspect is that entropy production accounted for in Equation (15) by the presence of the term $\dot{S}_i$ and one manifestation of this term in a thermo-plastically deforming material is

$$\dot{S}_i = \int_{\Omega_{ps}} \underline{q}_{ps} \cdot \nabla_{ps} \left(\frac{1}{T_{ps}} \right) dV_{ps} + \int_{\Omega_{ps}} \frac{\underline{\underline{\sigma}}_{ps} : \dot{\underline{\underline{\varepsilon}}}^{plas}_{ps}}{T_{ps}} dV_{ps} \tag{33}$$

Consider then Equation (10e) and the first term in Equation (33), which gives

$$\underline{q}_{ts} \cdot \nabla_{ts} \left(\frac{1}{T_{ts}} \right) = \alpha^s h \beta^3 \underline{q}_{ps} \cdot \nabla_{ps} \left(\frac{1}{T_{ps}} \right) \tag{34}$$

which is arrived at by first introducing the identity $\rho_{ts} \rho_{ts}^{-1}$ into Equation (33).

In view of $\underline{q}_{ts} = \alpha^e h \beta^2 \underline{q}_{ps}$ it can be deduced that Equation (34) reduces to

$$\alpha^e \nabla_{ts} \left(\frac{1}{T_{ts}} \right) = \alpha^s \beta \nabla_{ps} \left(\frac{1}{T_{ps}} \right) \tag{35}$$

which in view of Equation (32) and the identity reduces to $\nabla_{ts} = \beta \nabla_{ps}$, which is evidently consistent.

Consider now the application Equation (10e) and the second term in Equation (33), which gives

$$\frac{\underline{\underline{\sigma}}_{ts} : \dot{\underline{\underline{\varepsilon}}}^{plas}_{ts}}{T_{ts}} = \alpha^s h \beta^3 \frac{\underline{\underline{\sigma}}_{ps} : \dot{\underline{\underline{\varepsilon}}}^{plas}_{ps}}{T_{ps}} \tag{36}$$

which on substitution Equation (32) reduces to

$$\underline{\underline{\sigma}}_{ts} : \dot{\underline{\underline{\varepsilon}}}^{plas}_{ts} = \alpha^e h \beta^3 \underline{\underline{\sigma}}_{ps} : \dot{\underline{\underline{\varepsilon}}}^{plas}_{ps} \tag{37}$$

which is consistent with Equation (10e) accounting for energy sources and sinks.

A sink-like term in the energy equation can appear on application of the divergence theorem to the first term on the right hand side of Equation (14) to reveal

$$\int_{\Gamma_{ps}} \underline{v}_{ps} \cdot \underline{\underline{\sigma}}_{ps} \cdot \underline{n}_{ps} d\Gamma_{ps} = \int_{\Omega_{ps}} div\left(\underline{v}_{ps} \cdot \underline{\underline{\sigma}}_{ps}\right) dV_{ps} = \int_{\Omega_{ps}} \underline{v}_{ps} \cdot div\left(\underline{\underline{\sigma}}_{ps}\right) dV_{ps} + \int_{\Omega_{ps}} \nabla \underline{v}_{ps} : \underline{\underline{\sigma}}_{ps} dV_{ps} \qquad (38)$$

with the integrand in the last term equal to $\underline{\underline{\sigma}}_{ps} : \dot{\underline{\underline{\varepsilon}}}_{ps}^{elas} + \underline{\underline{\sigma}}_{ps} : \dot{\underline{\underline{\varepsilon}}}_{ps}^{plas}$, hence revealing the origin of Equation (37).

A more direct approach is to note from Equations (19) that (25) reveal that $\alpha^e = \alpha^\rho h^2 \beta^{-2}$, which gives $\underline{\underline{\sigma}}_{ts} = \alpha^e \beta^3 \underline{\underline{\sigma}}_{ps}$. Hence, it can be deduced from Equation (37) that $\dot{\underline{\underline{\varepsilon}}}_{ts}^{plas} = h \dot{\underline{\underline{\varepsilon}}}_{ps}^{plas}$, which is expected as direct differentiation of $\beta \underline{v}_{ts} = h \underline{v}_{ps}$ gives precisely $\dot{\underline{\underline{\varepsilon}}}_{ts} = h \dot{\underline{\underline{\varepsilon}}}_{ps}$.

6. REVERSE MAPPING

Established in Sections 4 and 5 is the existence of finite-similitude solutions for an isotropically scaled process. Finite similitude in this context is defined as the matching of scaled transport equations between physical and trial spaces. Essentially, a physical solution in the physical space is projected onto similar solutions in the trial space. Such solutions are known to exist as demonstrated in Section 5. However, an unfortunate side effect of the projection process can be projected-material behaviours that may not be reflected in any existing real material. An alternative viewpoint however is to start from a real material in the trial space and project this onto the physical space. In this case Equation (4) gives rise to

$$\frac{1}{g(t)} \frac{D^*}{D^* t} \int_{\Omega_{ps}^*} \rho_{ts} \psi_{ts} \left| F_{s^*}^{x^*} \right|^{-1} dV_{ps} + \int_{\Gamma_{ps}^*} \rho_{ts} \psi_{ts} \left| F_{s^*}^{x^*} \right|^{-1} F_{s^*}^{x^*} \otimes \left(\underline{v}_{ts} - \underline{v}_{ts}^*\right) \cdot \underline{n}_{ps} d\Gamma_{ps} =$$
$$- \int_{\Gamma_{ps}^*} \left| F_{s^*}^{x^*} \right|^{-1} F_{s^*}^{x^*} \otimes \underline{J}_{ts}^{\psi} \cdot \underline{n}_{ps} d\Gamma_{ps} + \int_{\Omega_{ps}^*} \rho_{ts} b_{ts}^{\psi} \left| F_{s^*}^{x^*} \right|^{-1} dV_{ps} \qquad (39)$$

which is proportional to Equation (3) after appropriate scalar multiplication to yield

$$\rho_{ps} \psi_{ps} = \alpha^{-\psi} \rho_{ts} \psi_{ts} \left| F_{s^*}^{x^*} \right|^{-1} \qquad (40a)$$

$$\underline{v}_{ps} - \underline{v}_{ps}^* = g F_{s^*}^{x^*} \otimes \left(\underline{v}_{ts} - \underline{v}_{ts}^*\right) \qquad (40b)$$

$$\underline{J}_{ps}^{\psi} = \alpha^{-\psi} g \left| F_{s^*}^{x^*} \right|^{-1} F_{s^*}^{x^*} \otimes \underline{J}_{ts}^{\psi} \qquad (40c)$$

and

$$\rho_{ps}^{\psi} b_{ps} = \alpha^{-\psi} g \rho_{ts} b_{ts}^{\psi} \left| F_{s^*}^{x^*} \right|^{-1} \qquad (40d)$$

and following the procedure outlined in Sections (4) and (5) a set of similarity relationships can be established.

The velocity of the control volumes is related by $\underline{v}^*_{ps} = gF^{x^*}_{s^*} \otimes \underline{v}^*_{ts} = g\beta\underline{v}^*_{ts}$ and similarly for material velocities, i.e. $\underline{v}_{ps} = gF^{x^*}_{s^*} \otimes \underline{v}_{ts} = g\beta\underline{v}_{ts}$. Continuity requirements lead to $\rho_{ps} = \alpha^{-\rho}\rho_{ts}\left|F^{x^*}_{s^*}\right|^{-1}$, which on substitution into Equations (40a) and (40d) give

$$\alpha^{-\rho}\psi_{ps} = \alpha^{-\psi}\psi_{ts} \tag{41a}$$

$$\alpha^{-\rho}b_{ps} = \alpha^{-\psi}gb^{\psi}_{ts} \tag{41d}$$

All the relationships identified in Section 5 hold although for a particular practical analysis $\alpha^{-\psi} \neq 1/\alpha^{\psi}$. However, the notation $\alpha^{-\psi}$ is chosen here to avoid the unnecessary replication of similarity relationships with different symbols.

7. TRANSPORT THEORY ON MATERIAL SPACES

As mentioned in Section 2 a somewhat circuitous route to scaling is through material spaces via a map between Ω_{TS} and Ω_{PS} or more correctly between control volumes Ω^*_{TS} and Ω^*_{PS}. The map is assumed to be isometric and gives rise to the relationship $\boldsymbol{dX}^* = F^{X^*}_{S^*} \otimes \boldsymbol{dS}^*$, where $F^{X^*}_{S^*} = \beta I$. Some care is needed when considering bodies described on a material space, which by choice and for convenience do not deform.

Consider then the movement of control volume Ω^*_{PS} over Ω_{PS} and whose motion is described by the velocity field $\underline{V}^*_{PS} = D^*\boldsymbol{X}^*/D^*t$. Somewhat peculiarly it is necessary to define a reference space for the reference space Ω^*_{PS}. A requirement brought about by a need to quantify the motion of Ω^*_{PS}. Consider then the diffeomorphism $\boldsymbol{X}^*(\boldsymbol{\chi},t)$, where $\underline{V}^*_{PS} = \partial\boldsymbol{X}^*/\partial t\big|_{\chi}$, and where $\boldsymbol{\chi}$ represents an arbitrary coordinate in the new reference space. Although Ω^*_{PS} has motion it is important to couple this to the motion of Ω^*_{ps} and more importantly not immediately rush to the direct formation of a transport equation for the control volume Ω^*_{PS} in the material space as any physics must arise from the physical space.

The map $\boldsymbol{X}^*(\boldsymbol{\chi},t)$ gives rise to the differential $d\boldsymbol{X}^* = F^{X^*}_{\chi} \otimes d\boldsymbol{\chi} + \underline{V}^*_{PS}dt$, where $F^{X^*}_{\chi} = \partial\boldsymbol{X}^*/\partial\boldsymbol{\chi}$ and $\underline{V}^*_{PS} = D^*\boldsymbol{X}^*/D^*t$. In view of the map $\boldsymbol{x}^*(\boldsymbol{X}^*,t):\Omega^*_{PS} \mapsto \Omega_{ps}$ and the associated differential $\boldsymbol{dx}^* = F^{x^*}_{X^*} \otimes \boldsymbol{dX}^* + \underline{v}^*_{ps}dt$ it follows that

$$\boldsymbol{dx}^* = F^{x^*}_{X^*}F^{X^*}_{\chi} \otimes \boldsymbol{d\chi} + \left(F^{x^*}_{X^*} \otimes \underline{V}^*_{PS} + \underline{v}^*_{ps}\right)dt = F^{x^*}_{\chi} \otimes \boldsymbol{d\chi} + \underline{V}^{rel}dt \tag{42}$$

where $F^{x^*}_{\chi} = \partial\boldsymbol{x}^*/\partial\boldsymbol{\chi} = F^{x^*}_{X^*}F^{X^*}_{\chi}$, and where

$$\underline{V}^{rel} = \frac{D^*\boldsymbol{x}^*}{D^*t} = F^{x^*}_{X^*} \otimes \underline{V}^*_{PS} + \underline{v}^*_{ps} \tag{43}$$

The existence of the map $\boldsymbol{x}^*\left(\boldsymbol{X}^*,t\right):\Omega^*_{PS}\mapsto\Omega_{ps}$ and associated differential $\boldsymbol{dx}^*=F^{x^*}_{X^*}\otimes\boldsymbol{dX}^*+\underline{v}^*_{ps}dt$ gives rise to the Nanson's identities $dV_{ps}=\left|F^{x^*}_{X^*}\right|dV_{PS}$ and $\underline{d\Gamma}^*_{ps}=\left|F^{x^*}_{X^*}\right|\underline{d\Gamma}^*_{PS}\otimes\left(F^{x^*}_{X^*}\right)^{-1}$, where dV_{PS} is an elemental volume in Ω^*_{PS} (and hence Ω_{PS}) and $\underline{d\Gamma}^*_{PS}=\underline{N}^*_{PS}d\Gamma^*_{PS}$ with $\underline{N}^*_{PS}$ being an outward pointing unit normal on Γ^*_{PS} the boundary of Ω^*_{PS}. Substitution of these identities into Equation (3) gives rise to a transport equation on the material reference space, i.e.

$$\frac{D^*}{D^*t}\int_{\Omega^*_{PS}}\rho_{ps}\psi_{ps}\left|F^{x^*}_{X^*}\right|dV_{PS}+\int_{\Gamma^*_{PS}}\rho_{ps}\psi_{ps}\left|F^{x^*}_{X^*}\right|\left(F^{x^*}_{X^*}\right)^{-1}\otimes\left(\underline{v}_{ps}-\underline{v}^*_{ps}\right)\cdot\underline{N}^*_{PS}d\Gamma^*_{PS}=$$
$$-\int_{\Gamma^*_{PS}}\left|F^{x^*}_{X^*}\right|\left(F^{x^*}_{X^*}\right)^{-1}\otimes\underline{J}^{\psi}_{ps}\cdot\underline{N}^*_{PS}d\Gamma^*_{PS}+\int_{\Omega^*_{PS}}\rho_{ps}b^{\psi}_{ps}\left|F^{x^*}_{X^*}\right|dV_{PS}\qquad(44)$$

It follows that the same apparatus can be replicated for the trial space with Equation (6) replicating Equation (4) and transforming into

$$\frac{D^*}{D^*\tau}\int_{\Omega^*_{TS}}\rho_{ts}\psi_{ts}\left|F^{s^*}_{S^*}\right|dV_{TS}+\int_{\Gamma^*_{TS}}\rho_{ts}\psi_{ts}\left|F^{s^*}_{S^*}\right|\left(F^{s^*}_{S^*}\right)^{-1}\otimes\left(\underline{v}_{ts}-\underline{v}^*_{ts}\right)\cdot\underline{N}^*_{TS}d\Gamma^*_{TS}=$$
$$-\int_{\Gamma^*_{TS}}\left|F^{s^*}_{S^*}\right|\left(F^{s^*}_{S^*}\right)^{-1}\otimes\underline{J}^{\psi}_{ts}\cdot\underline{N}^*_{TS}d\Gamma^*_{TS}+\int_{\Omega^*_{TS}}\rho_{ts}b^{\psi}_{ts}\left|F^{s^*}_{S^*}\right|dV_{TS}\qquad(45)$$

where time scales in the trial and physical space are related in the usual way by $dt=h(\tau)d\tau$ or $d\tau=g(t)dt$, where $h(\tau)g(t)=1$.

Equations (44) and (45) are essentially independent but for similar systems can be related via scaling with $\boldsymbol{dX}^*=F^{X^*}_{S^*}\otimes\boldsymbol{dS}^*$, where $F^{X^*}_{S^*}=\beta I$ and the associated Nanson's identities $dV_{PS}=\left|F^{X^*}_{S^*}\right|dV_{TS}$ and $\underline{d\Gamma}^*_{PS}=\left|F^{X^*}_{S^*}\right|\underline{d\Gamma}^*_{TS}\otimes\left(F^{X^*}_{S^*}\right)^{-1}$. Substitution into Equation (44) along with time rescaling gives

$$\frac{1}{h(\tau)}\frac{D^*}{D^*\tau}\int_{\Omega^*_{TS}}\rho_{ps}\psi_{ps}\left|F^{x^*}_{X^*}\right|\left|F^{X^*}_{S^*}\right|dV_{TS}+\int_{\Gamma^*_{TS}}\rho_{ps}\psi_{ps}\left|F^{x^*}_{X^*}\right|\left|F^{X^*}_{S^*}\right|\left(F^{x^*}_{X^*}\right)^{-1}\left(F^{X^*}_{S^*}\right)^{-1}\otimes\left(\underline{v}_{ps}-\underline{v}^*_{ps}\right)\cdot\underline{N}^*_{TS}d\Gamma^*_{TS}=$$
$$-\int_{\Gamma^*_{TS}}\left|F^{x^*}_{X^*}\right|\left|F^{X^*}_{S^*}\right|\left(F^{x^*}_{X^*}\right)^{-1}\left(F^{X^*}_{S^*}\right)^{-1}\otimes\underline{J}^{\psi}_{ps}\cdot\underline{N}^*_{TS}d\Gamma^*_{TS}+\int_{\Omega^*_{TS}}\rho_{ps}b^{\psi}_{ps}\left|F^{x^*}_{X^*}\right|\left|F^{X^*}_{S^*}\right|dV_{TS}\qquad(46)$$

which on multiplication by $h(\tau)$ and α^{ψ}, and matching of integrands with Equation (45) yields

$$\rho_{ts}\psi_{ts}\left|F^{s^*}_{S^*}\right|=\alpha^{\psi}\rho_{ps}\psi_{ps}\left|F^{x^*}_{X^*}\right|\left|F^{X^*}_{S^*}\right|\qquad(47a)$$

$$\left|F_{S^*}^{s^*}\right|\left(F_{S^*}^{s^*}\right)^{-1}\otimes\left(\underline{v}_{ts}-\underline{v}_{ts}^{*}\right)=h\left|F_{X^*}^{x^*}\right|\left|F_{S^*}^{X^*}\right|\left(F_{X^*}^{x^*}\right)^{-1}\left(F_{S^*}^{X^*}\right)^{-1}\otimes\left(\underline{v}_{ps}-\underline{v}_{ps}^{*}\right) \tag{47b}$$

$$\left|F_{S^*}^{s^*}\right|\left(F_{S^*}^{s^*}\right)^{-1}\otimes\underline{J}_{ts}^{\psi}=\alpha^{\psi}h\left|F_{X^*}^{x^*}\right|\left|F_{S^*}^{X^*}\right|\left(F_{X^*}^{x^*}\right)^{-1}\left(F_{S^*}^{X^*}\right)^{-1}\otimes\underline{J}_{ps}^{\psi} \tag{47c}$$

and

$$\left|F_{S^*}^{s^*}\right|\rho_{ts}^{\psi}b_{ts}=\alpha^{\psi}h\rho_{ps}b_{ps}^{\psi}\left|F_{X^*}^{x^*}\right|\left|F_{S^*}^{X^*}\right| \tag{47d}$$

where setting $\left|F_{S^*}^{s^*}\right|\left(F_{S^*}^{s^*}\right)^{-1}\otimes\underline{v}_{ts}=h\left|F_{X^*}^{x^*}\right|\left|F_{S^*}^{X^*}\right|\left(F_{X^*}^{x^*}\right)^{-1}\left(F_{S^*}^{X^*}\right)^{-1}\otimes\underline{v}_{ps}$ and $\left|F_{S^*}^{s^*}\right|\left(F_{S^*}^{s^*}\right)^{-1}\otimes\underline{v}_{ts}^{*}=h\left|F_{X^*}^{x^*}\right|\left|F_{S^*}^{X^*}\right|\left(F_{X^*}^{x^*}\right)^{-1}\left(F_{S^*}^{X^*}\right)^{-1}\otimes\underline{v}_{ps}^{*}$ is sufficient for Equation (47b).

Contrasting Equation (47) with Equation (7) reveals that they are identical if and only if $F_{S^*}^{s^*}=F_{X^*}^{x^*}$ since by default $F_{S^*}^{X^*}=F_{s^*}^{x^*}=\beta I$. The requirement that $F_{S^*}^{s^*}=F_{X^*}^{x^*}$ is a direct consequence of $\left|F_{S^*}^{s^*}\right|\left(F_{S^*}^{s^*}\right)^{-1}\otimes\underline{v}_{ts}^{*}=h\left|F_{X^*}^{x^*}\right|\left|F_{S^*}^{X^*}\right|\left(F_{X^*}^{x^*}\right)^{-1}\left(F_{S^*}^{X^*}\right)^{-1}\otimes\underline{v}_{ps}^{*}$ matching $\underline{v}_{ts}^{*}=h\left(F_{s^*}^{x^*}\right)^{-1}\otimes\underline{v}_{ps}^{*}$, which a necessary condition for the synchronisation of control volume movement.

It can be concluded therefore that scaling via material spaces is possible and feasible and if correctly interpreted yields the exact same information as direct scaling in the physical space. It is worth noting that Equation (44) provides a transport equation in the material space of the form

$$\frac{D^*}{D^*t}\int_{\Omega_{PS}^*}\rho_{PS}\Psi_{PS}dV_{PS}+\int_{\Gamma_{PS}^*}\rho_{PS}\Psi_{PS}\left(\underline{V}_{PS}-\underline{V}_{PS}^{*}\right)\cdot\underline{N}_{PS}^{*}d\Gamma_{PS}^{*}=$$
$$-\int_{\Gamma_{PS}^*}\underline{J}_{PS}^{\psi}\cdot\underline{N}_{PS}^{*}d\Gamma_{PS}^{*}+\int_{\Omega_{PS}^*}\rho_{PS}b_{PS}^{\psi}dV_{PS} \tag{48}$$

which erroneously suggests that material movement with velocity $\underline{V}_{PS}$ takes place on the material domain. This illustrates the need to treat equations in the material reference space with a certain degree of caution since by default no motion takes place in the material reference frame.

8. THE ROLE OF CONSTITUTIVE LAWS

The foundational similarity conditions established in Section 3 have Equation (7c) (along with Equation (10d) in Section 4) providing the link between flux transfers taking place in the trial and physical spaces. Equation (7c) effectively provides information on the transfer mechanisms that are taking place at the boundary of a domain but closure for solution of the transport equations is required. A feature of similarity however is proportional transfers but modern-analysis approaches utilise constitutive laws, which generally are unlikely to scale. In the case of momentum transfer, traction is associated with applied force but for stress to develop in a body, material deformation must occur. Stress is typically related continuously

to strains, strain rates and temperature and an expression pertinent to metal forming is (amongst many others) is the Johnson-Cook expression [16],

$$\bar{\sigma}_{ps} = \left(Y_{ps} + B_{ps}\bar{\varepsilon}_{ps}^{n}\right)\left(1 + C\ln\left(\frac{\dot{\bar{\varepsilon}}_{ps}}{\dot{\bar{\varepsilon}}_{ps}^{0}}\right)\right)\left(1 - \left(\frac{T_{ps} - T_{ps}^{0}}{T_{ps}^{0}}\right)^{m}\right) \tag{49}$$

where Y_{ps} is the initial yield stress, $\dot{\bar{\varepsilon}}_{ps}^{0}$ is a reference strain rate, T_{ps}^{0} is a reference temperature and *B, n, C* and *m* are coefficients determined by experimental means.
In view of the identity $\bar{\sigma}_{ts} = \alpha^{\rho}h^{2}\beta\bar{\sigma}_{ps}$, established in Section 5.2 and the proportional relationships for temperature and strain rate with strain being dimensionless, Equation (49) transforms into

$$\bar{\sigma}_{ts} = \left(Y_{ts} + B_{ts}\bar{\varepsilon}_{ts}^{n}\right)\left(1 + C\ln\left(\frac{\dot{\bar{\varepsilon}}_{ts}}{\dot{\bar{\varepsilon}}_{ts}^{0}}\right)\right)\left(1 - \left(\frac{T_{ts} - T_{ts}^{0}}{T_{ts}^{0}}\right)^{m}\right) \tag{50}$$

where $Y_{ts} = \alpha^{\rho}h^{2}\beta Y_{ps}$, $B_{ts} = \alpha^{\rho}h^{2}\beta B_{ps}$, $\bar{\varepsilon}_{ts} = \bar{\varepsilon}_{ps}$ and $\dot{\bar{\varepsilon}}_{ts} = h\dot{\bar{\varepsilon}}_{ps}$.
Equation (50) provides the material response necessary for material similarity but it is possible that the particular material response may not in fact exist in a ready available material. However, provided with a physical material (that approximates this material in some sense) for use in the trial space, the reverse mapping then provides information about the behaviour of the material in the physical space. Other material properties of interest to thermo-mechanical analysis is thermal conductivity and with application of a classical Fourier law $\underline{q}_{ps} = -K_{ps}\nabla_{ts}T_{ps}$ but for similarity $\underline{q}_{ts} = \alpha^{e}h\beta^{2}\underline{q}_{ps}$ and $\nabla_{ts} = \beta\nabla_{ps}$, and since $\alpha^{s}T_{ts} = \alpha^{e}T_{ps}$, it follows that

$$K_{ts} = \alpha^{s}h\beta K_{ps} \tag{51}$$

which may or may not match the behaviour of a selected trial space material.
However, as mentioned above, projection between physical and trial spaces cuts both ways making it possible to gauge the importance of any mismatch in material properties. It is thus of interest to explore this aspect further to ascertain the practical benefits and limitations of the similarity approach.

9. PRACTICAL PROCEDURES AND CONSTRAINTS

Despite the apparent mathematical complexity associated with the development of the finite-similitude theory its application is relatively straightforward. In the case of isotropic scaling (i.e. $F_{s^*}^{X^*} = \beta I$ or $F_{S^*}^{X^*} = \beta I$) there are 7 scalar scaling parameters in total, which are: β, h, α^{ρ}, α^{v}, $\alpha^{\underline{u}}$, α^{e} and α^{s}. The scaling factors are not completely independent and the dependencies are re-presented here for convenience:

- The velocity scaling factor is dependent and related to time, geometry and the density scaling through the relationship $\alpha^{v} = h\alpha^{\rho}/\beta$.

- The displacement scaling factor is dependent and related to velocity and time scaling by $\alpha^{\underline{u}} = \alpha^{\underline{v}}/h = \alpha^{\rho}/\beta$.
- The energy scaling factor is dependent and related to velocity and density scaling by $\alpha^{e} = \left(\alpha^{\underline{v}}\right)^2 / \alpha^{\rho}$.

Accounting for these three dependencies reveals four independent scaling factors. There is however a number of different possible combinations of independent scaling factors. An upper bound on the number of combination is $C_4^7 = 35$ but in practice the three dependencies along with practical limitations lowers significantly the number of realistic choices. In a situation where similitude is approximate then different choices can produce different outcomes. Consider for example the independent scaling factors for geometry, time, density and entropy, i.e. $\left\{\beta, h, \alpha^{\rho}, \alpha^{s}\right\}$ as listed in Table 1. The consequences of this choice on dependent and independent physical quantities are presented in Tables 1 and 2.

Table 1. Independent scaling factors.

Scaling factor	β	α^{ρ}	h	α^{s}
Equation No.		(16)	(20)	(32)
Relationship	l_{ps}/l_{ts}	$\beta^{-3}\,\rho_{ts}/\rho_{ps}$	$\beta\sqrt{\left(\rho_{ps}/\rho_{ts}\right)\left(Y_{ts}/Y_{ps}\right)}$	$\beta^{-3}\left(Y_{ts}/Y_{ps}\right)\left(T_{ps}/T_{ts}\right)$
Quantity affected	l_{ts}	ρ_{ts}	Y_{ts}	T_{ts}

Table 2. Dependent scaling factors.

Scaling factor	$\alpha^{\underline{u}}$	$\alpha^{\underline{v}}$	α^{e}
Equation No.	(22)	(19)	(25)
Relationship	$\beta^{-1}\alpha^{\rho}$	$h\beta^{-1}\alpha^{\rho}$	$h^2\beta^{-2}\alpha^{\rho}$
Field influenced	$\underline{u}_{ts}$	$\underline{v}_{ts}$	u_{ts}

The physical quantities in the bottom row in Table 1 are principally affected by the choice of independent factors. Thus for example the selection of α^{ρ} as an independent scaling factor prescribes the initial value of density ρ_{ts} given that β and ρ_{ps} are prescribed. Similarly Table 2 presents how values of dependent-scaling factors influence the physical fields of displacement, velocity and specific internal energy. The dependent factors are determined to ensure that the associated physical quantities are in the correct proportions with the physical space.

The first four steps of a procedure for designing scaled experiments (called ***direct scaling***) is as follows:

- Select the material (or materials) to be used in the scaled experiment. The associated model is referred to here as the *trial model*.
- Select the independent scaling factors (a choice generally influenced by the dominant physics) and determine their values.
- Determine the values of the dependent scaling factors.
- Use the scaling factors to calculate physical parameters and material properties for the scaled model; referred to here as the *direct scaled model*. Note that in the absence of finite similitude the trial and direct scaled models will not match.

To illustrate the procedure consider a full-scale steel (subscript *St*) model and an aluminium (subscript *Al*) trial model along with scaling relationships presented in Tables 1 and 2. The important scaled material parameters are identified and in this case are selected to be density, yield stress and temperature. With the geometric scaling parameter β set, the selected scaled model parameters are also fixed, i.e. $\rho_{ts} = \rho_{Al}$, $Y_{ts} = Y_{Al}$ and the initial temperature $T_{ts}^{initial} = T^{room}$, where T^{room} is the initial room temperature, which can be a cost-effective choice for any material used in a laboratory setting. This information immediately determines the independent and dependent scaling factors, which are provided in symbolic form in Tables 3 and 4.

Table 3. Independent scaling factors for aluminium as trial material.

Scaling factor	β	α^{ρ}	h	α^{s}
Equation No.		(16)	(20)	(32)
Relationships	specified	$\beta^{-3}\left(\rho_{Al}/\rho_{St}\right)$	$\beta\sqrt{\left(\rho_{St}/\rho_{Al}\right)\left(Y_{Al}/Y_{St}\right)}$	$\beta^{-3}\left(Y_{Al}/Y_{St}\right)\left(T_{St}/T_{room}\right)$

Table 4. Dependent scaling factors for aluminium as a trial material

Scaling factor	$\alpha^{\underline{u}}$	$\alpha^{\underline{v}}$	α^{e}
Equation No.	(22)	(19)	(25)
Relationship	$\beta^{-4}\left(\rho_{Al}/\rho_{St}\right)$	$h\beta^{-4}\left(\rho_{Al}/\rho_{St}\right)$	$h^2\beta^{-5}\left(\rho_{Al}/\rho_{St}\right)$

The values of dependent and independent scaling factors (Tables 3 and 4) together facilitate the creation of a scaled material model, which can be viewed as a virtual material. This material will possess other material properties as a consequence of the choices made in these tables. A selection of the material properties for the virtual material is tabulated in symbolic form in Table 5.

Table 5. Scaled material constants dictated by scaling factors.

	Young's modulus	Thermal conductivity	Johnson-Cook strain-hardening coefficient	Melting temperature
Quantity	E_{ts}	K_{ts}	B_{ts}	T_{ts}^{melt}
Relationship	$\alpha^{\rho}h^2\beta E_{ps}$	$\alpha^{s}h\beta K_{ps}$	$\alpha^{\rho}h^2\beta B_{ps}$	$\left(\alpha_e/\alpha_s\right)T_{ps}^{melt}$
Symbolic value	$\left(Y_{Al}/Y_{St}\right)E_{St}$	$\sqrt{\left(\rho_{St}/\rho_{Al}\right)\left(Y_{Al}/Y_{St}\right)^3}$ $\times\beta^{-1}\left(T_{ps}/T_{room}\right)K_{St}$	$\left(Y_{Al}/Y_{St}\right)B_{St}$	$\left(T_{room}/T_{ps}\right)T_{St}^{melt}$

It can be expected that the virtual material will generally differ from the selected trial material model (Aluminium) although by choice $\{\rho_{ts}, Y_{ts}\}$ match $\{\rho_{Al}, Y_{Al}\}$. Loading conditions/process parameters for the scaled experiment are dictated by the parameters provided in Tables 1 and 2 in a similar fashion and relationships for time, displacement and strain rate are provided in Table 6.

Table 6. Scaled experiment loading conditions dictated by scaling factors.

Quantity	Process time	Axial displacement	Loading strain rate
Symbol	τ^{elapse}	$\underline{u}_{ts}^{applied}$	$\dot{\varepsilon}_{ts}^{loading}$
Relationship	$\tau^{elapse} = h^{-1}t^{elapse}$	$\left(\alpha^{\underline{u}}/\alpha^{\rho}\right)\underline{u}_{ps}^{applied}$	$h\dot{\varepsilon}_{ps}^{loading}$

It is possible to identify other parameters of the trial and direct-scaled model rather than simply focus on material properties. For example, with a dynamic thermo-mechanical full-scale model, it may be possible and sufficient to consider a quasi-static scaled experiment, which will lead to a different outcome to those presented in Tables 3 to 6. The ability to focus on important parameters is an important feature of the procedure but an equally important aspect is the ability to gauge the effect of these choices at the full scale.

To replicate the results of the scaled experiment in the full-scale space, the *reverse scaling maps* (see Section 6) apply to the real scaled experiment, which consists of the trial material model (Aluminium in this case) and scaled loading conditions (Table 6). The resulting material model is called the *reversed trial material* which in general will differ from the full-scale material model except for the identified matched parameters. One aspect that is assured, however, is that the virtual scaled material model under reverse scaling is identical to the full-scale material model (e.g. Steel in this case).

It is possible to consider a procedure that adjusts scaling factors in such a manner that minimises some objective function quantifying differences between the virtual and real behaviours. This aspect is just mentioned in passing here but the fact that errors/differences can be identified is important information in its own right as known differences can often be accounted for and accommodated in any experimental trial.

10. NUMERICAL EXPERIMENTS

This section introduces a number of case studies with specific features to provide a proof of concept and to test out the new scaling theory. Case Study I is a pure thermal process with sufficient independent scale factors to provide finite similitude on scaling. This is followed by a purely mechanical metal forming process where iteration is required to get a good approximation. The final case study presents a thermo-mechanical analysis, where different trial materials are considered but yet again reasonable mechanical behaviour is shown possible. Overall the effect of parameter selection is examined in this section through different thermal, mechanical and thermo-mechanical numerical simulations. The numerical analyses are performed using the commercial finite element software ABAQUS [17]. It is important to appreciate however that the theory presented in the previous sections sits above any analysis therefore allowing for the application of any form of analysis (e.g. numerical/analytical) and code (e.g. commercial/bespoke). A consistent system of units is used for the numerical experiments, which are: *kg, mm, ms, K, kN, GPa*, *J* and *kW*, respectively for the mass, length, time, temperature, force, stress, energy and power.

10.1 CASE STUDY I: PURE THERMAL PROCESS

In this case study, heat transfer through a steel cuboid with dimensions $10mm \times 10mm \times 100mm$ is considered as the full-scale model. Spatially uniform and temporally constant uniform heat

fluxes $q_{ps} = 10^{-3}\, kW/mm^2$ are applied through rectangular faces with a fixed temperature $T_{ps} = 400K$ boundary condition on the square ends (see Figure 2). The transient analysis using 8-noded convection/diffusion brick elements (DCC3D8D) is performed in the ABAQUS Heat Transfer environment. The full-scale model process time t^{elapse} is equal to $1000ms$ and its associated physical properties are: $\rho_{ps} = 7.83\times10^{-6} kg\ mm^{-3}$, $K_{ps} = 4.45\times10^{-5} kWmm^{-1}K^{-1}$ and $c_{ps} = 475J\ kg^{-1}K^{-1}$ for density, thermal conductivity and specific heat capacity, respectively [18]. Aluminium is selected as the trial material model with thermal material properties: $\rho_{ts} = 2.77\times10^{-6} kg\ mm^{-3}$, $K_{ts} = 14\times10^{-5} kWmm^{-1}K^{-1}$ and $c_{ts} = 880J\ kg^{-1}K^{-1}$ [18]. Using the direct scaling maps involved in this problem, the independent scaling factors are listed in Table 7.

Table 7. Independent scaling factors of Case Study I.

Scaling factor	α^{ρ}	α^{s}	h
Equation No.	(16)	(26), (32)	(51)
Relationship	$\beta^{-3}\rho_{ts}/\rho_{ps}$	$\left(c_{ts}/c_{ps}\right)\alpha^{\rho}$	$\beta^{-1}\left(K_{ts}/K_{ps}\right)\left(1/\alpha^{s}\right)$
Quantity affected	ρ_{ts}	c_{ts}	K_{ts}

Table 8. Case Study I: scaled experiment dependent design parameters.

Quantity	Process time τ^{elapse} $[ms]$	Energy scaling factor α^{e}	Initial temperature $T_{ts}^{initial}$ $[K]$	Applied heat loading $q_{ts}^{applied}$ $[kW/mm^2]$
Equation No.	---	(19),(25)	(32)	(10d)
Relationship	$h^{-1}t^{elapse}$	$h^2\beta^{-2}\alpha^{\rho}$	$\left(\alpha^{e}/\alpha^{s}\right)T_{ps}^{initial}$	$\alpha^{e}h\beta^{2}q_{ps}^{applied}$
Numerical value	3333.1	32.60	310.93	0.611×10^{-3}

The direct scaling independent factors are given in Table 7 and dictate the value of the dependent scaling factor α^{e} and the loading conditions as presented in Table 8. A feature of this case study is that the number of independent scaling factors is equal to the number of physical variables. Therefore all the scaled material properties are free to be set equal to the properties of the trial material model (see Table 3). To see how the scaled trial-model results are replicated in the full-scale space, they are transferred to the physical space. For this purpose the trial model temperature and z-coordinate should be multiplied by the reverse scaling factors as illustrated in Figure 3. An exact agreement between the spatial distribution of temperature along the central longitudinal path in the full-scale and reversed trial experiments is depicted in Figure 3. The predictions in Figure 3 are in accordance with the theory (see Sections 5-6) with an exact replication of the scaled model at the full scale. This is an example of finite similitude, which is seldom expected for more complex problems. It is in situations where finite similitude does not exist that the new approach offers the possibility of reasonably good approximations, as examined in Case Studies II and III.

10.2 CASE STUDY II: PURE MECHANICAL PROCESS

An open die cold forging of a cylinder is considered as the second case study. The dimensions of the full-scale model are 40*mm* in diameter and 60*mm* in length deformed in the axial direction to one-fourth of its original length. The dimensional scaling factor β is set to be 2 and consequently the initial dimensions of the scaled model are 20*mm* and 30*mm* for diameter and length respectively. The full-scale model is made of aluminium 7039 with mechanical properties and Johnson-Cook constitutive relation coefficients (see Equation (49)) presented in Table 9. The material model is taken to be elastic-plastic, with Young's modulus and Poisson's ratio also provided in Table 9.

Table 9. Full-scale and scaled experiments material constants [18].

Material	ρ $[kg/mm^3]$	E $[GPa]$	ν	Y $[GPa]$	B [$[GPa]$	n	C	$\dot{\bar{\varepsilon}}^0$ $[(ms)^{-1}]$
PS: Al 7039	2.77×10^{-6}	70	0.33	0.337	0.343	0.41	0.010	1×10^{-3}
TS: Steel 4340	7.83×10^{-6}	200	0.3	0.792	0.510	0.26	0.014	1.8×10^{-3}
TS: Steel 1006	7.89×10^{-6}	210	0.3	0.350	0.275	0.36	0.022	1.2×10^{-3}

Cold forging is assumed to be a pure mechanical phenomenon, so can be reasonably approximated to be isothermal, i.e. $T_{ps} = T_{ts} = T_0$. This condition on examination of Equation (32) reveals that the entropy scaling factor α^s is not an independent design factor, i.e. $\alpha^s = \alpha^e$. Therefore the number of free independent scaling factors for this case study is three, i.e. β, h and α^ρ. Setting $\beta = 2$ dictates that the total axial displacement u_{ts}^{axial} of the scaled experiment, which is equal to $u_{ps}^{axial} \big/ \beta = 7.5mm$. More details on the geometry, mesh and loading conditions for the full and scaled models is provided in Figure 4.

Two different possible designs (termed Designs I and II) for the scaled experiments are studied such that in Design I, density ρ_{ts} and yield stress Y_{ts} are set to be equal to the trial material values, whilst in Design II, density ρ_{ts} and strain hardening coefficient B_{ts} of the scaled models are fixed. Each design is tested for two different material models (Steel 4340 and Steel 1006) as possible trial materials (termed Trial I and Trial II).

10.2.1 Design I

Since there are only two independent factors for this case, the density and yield stress of the scaled material are fixed and set equal to the trial material values as the first design of the scaled experiment. Steel 4340 is selected as the first trial material model with $\rho_{ts} = \rho_{\text{steel 4340}}$ and $Y_{ts} = Y_{\text{steel 4340}}$, and the scaling factors for this situation are: $h = 1.823$, $\alpha^\rho = 0.353$, $\alpha^v = 0.322$, $\alpha^u = 0.17$ and $\alpha^e = \alpha^s = 0.294$. The full-scale and replicated scaled numerical results for axial load versus displacement are shown in Figure 5. For the second trial material, Steel 1006 is selected with $\rho_{ts} = \rho_{\text{steel 1006}}$ and $Y_{ts} = Y_{\text{steel 1006}}$. The scaling factors in this case are: $h = 1.207$, $\alpha^\rho = 0.356$, $\alpha^v = 0.215$, $\alpha^u = 0.17$ and $\alpha^e = \alpha^s = 0.13$, with results for axial load versus displacement depicted in Figure 6.

10.2.2 Design II

For the second design of the scaled experiment, the density and strain hardening coefficient of the scaled material are set equal to the trial material density and its strain hardening coefficient, respectively, i.e. $\rho_{ts} = \rho_{\text{steel 4340}}$ and $B_{ts} = B_{\text{steel 4340}}$ in the first trial $\rho_{ts} = \rho_{\text{steel 1006}}$ and $B_{ts} = B_{\text{steel 1006}}$ in the second trial. The scaling factors for Steel 4340 as the trial material model are calculated as: $h = 1.45$, $\alpha^{\rho} = 0.353$, $\alpha^{\underline{v}} = 0.256$, $\alpha^{\underline{u}} = 0.17$ and $\alpha^{e} = \alpha^{s} = 0.186$ and corresponding results can be found in Figure 7. Similarly, for the second trial with Steel 1006 as the trial material the factors are: $h = 1.06$, $\alpha^{\rho} = 0.356$, $\alpha^{\underline{v}} = 0.189$, $\alpha^{\underline{u}} = 0.17$ and $\alpha^{e} = \alpha^{s} = 0.10$. The results for this case again for axial load versus displacement are depicted in Figure 8.

Comparison between the results (see Figures 5 to 8) of Designs I and II highlights the variability in predictions as a consequence of matching of different physical parameters. The results of the reversed trial model of Design I replicate closer the data to the full-scale results. The reason for this is that for a simple upsetting problem the sensitivity of the results depends critically on the yield stress, which is matched in Design I. The targeting of strain hardening in Design II transpires to be a less effective strategy and the outcome highlights the importance of physical insight.

10.3 CASE STUDY III: THERMO-MECHANICAL PROCESS

In this section hot forging of a cylinder is considered as a thermo-mechanical case study. The dimensions of the full-scale physical model are diameter $D_{ps} = 30\,mm$ and length $\ell_{ps} = 30$ *mm*. The dimensional scaling factor β is set to be 2 and therefore the dimensions of the scaled trial model are $D_{ts} = 15\,mm$ and $\ell_{ts} = 15\,mm$. The process is thermo-mechanical and consists of raising the temperature (an initiating step) of the full-scale model to 700*K* and then applying axial displacement by amount of $\ell_{ps}^{axial}/2$ for the full-scale model (correspondingly $\ell_{ts}^{axial}/2$ for the scaled model). The details of geometry, mesh and thermomechanical boundary conditions for the full and scaled experiments models can be found in Figure 9.

The natural heat convection between the surface of the cylinder and the surrounding area (dry air) is modelled during step 2. The time process of the unscaled model for the initiating step is 0.01*ms* and for subsequent deformation is 1*ms*, i.e. a high-loading rate typical to impact forming is considered. The corresponding process times for the scaled model depend on the selected trial material, i.e. time scaling factor *h* (with *h* considered dependent). The full-scale billet is made of Steel 4340 with the mechanical properties presented in Table 9 and thermal properties as: thermal conductivity $K = 4.45\times10^{-5}\,kWmm^{-1}K^{-1}$, specific heat capacity $c = 475J\ kg^{-1}K^{-1}$, thermal expansion coefficient $\alpha_{\text{exp}} = 1.23\times10^{-5}K^{-1}$, $m = 1.03$, $T^{melt} = 1793K$ and $T^{0} = 293K$ for Johnson-Cook relation thermal constants [18] as presented in Equation (49).

Two possibilities are considered for the trial materials. In the first trial model the behaviour of aluminium 7039 is adopted as the trial material model with the mechanical properties presented in Table 9 and its related thermal constants $K = 1.40\times10^{-5}\,kWmm^{-1}K^{-1}$,

$c = 880 J\ kg^{-1}K^{-1}$, $\alpha_{\exp} = 2.34\times10^{-5}K^{-1}$, $m = 1$, $T^{melt} = 877K$ and $T^{0} = 293K$ [18]. A tungsten alloy (0.07Ni, 0.03Fe) is considered as the second trial material model. The material properties and Johnson-Cook coefficients for the selected tungsten alloy are: $\rho = 1.70\times10^{-5} kg\ mm^{-3}$, $E = 450GPa$, $\nu = 0.28$, $Y = 1.506GPa$, $B = 0.177GPa$, $\dot{\varepsilon}^{0} = 0.1ms^{-1}$, $C = 0.016$, $n = 0.12$, $m = 1$, $T^{melt} = 1723K$, $T^{0} = 293K$, $c = 134 J\ kg^{-1}K^{-1}$, $K = 1\times10^{-4} kWmm^{-1}K^{-1}$, $\alpha_{\exp} = 5\times10^{-6}K^{-1}$. There are 4 independent scaling factors in this problem and consequently the density, yield stress and initial temperature of the scaled model are fixed, i.e. $\rho_{ts} = \rho_{\text{trial mat}}$, $Y_{ts} = Y_{\text{trial mat}}$ and $T_{ts}^{initial} = T^{room}$. Based on the selected trial material models and the design conditions, the direct scaling factors are determined and the numerical values are presented in Table 10.

Table 10. Scaling factors of Case Study III

Factor	β	h	α^{ρ}	$\alpha^{\underline{v}}$	$\alpha^{\underline{u}}$	α^{e}	α^{s}
Al 7039	2	2.19	0.044	0.048	0.0219	0.053	0.127
Tungsten	2	1.87	0.027	0.025	0.013	0.238	0.568

These scaling factors dictate the following loading conditions for the scaled experiments where μ and h_{conv}, represents the friction and convection film coefficients, respectively. The loading conditions necessary for numerical simulation of the scaled experiment using two trial material models is provided in Tables 11. Using the given information in Table 10, the results of the scaled experiment models can be transferred to the physical space through reverse scaling maps. The replicated results of the scaled model and the full-scale model behaviour for axial force-displacement are compared in Figure 10.

Table 11. Scaled experiments loading conditions for Case Study III

Quantity	Process time $[ms]$	Total axial displacement u^{axial} $[mm]$	Initial temperature $T^{initial}$ $[K]$	Coefficient of friction μ	Heat transfer coefficient h_{conv} $[kW/mm^2K]$
PS: Steel 4340	1	15	700	0.6	5×10^{-8}
TS: aluminium	0.455	7.5	293	0.6	5.57×10^{-8}
TS: tungsten	0.534	7.5	293	0.6	5×10^{-8}

The zoomed area in Figure 10 illustrates that the both reversed scaled models initiate the plastic yielding at the same point as the full-scale model. This feature is a consequence of matching the yield stress of both trial models with the full scale model. Thus as anticipated, under reversed scaling, the two yield stresses match with the full-scale material. In order to gauge how the geometry behaves the temporal variation of the meridian circle radius for the two scaled experimental models and their reversed replications are presented in Figure 11, where high accuracy is observed. It is of interest to observe the change of temperature predicted by the scaled experiments at full scale. The spatial distribution of temperature distribution of trial models, full-scale and reversed scaled models at final stage of the process are depicted in Figure 12, respectively. The spatial and temporal variations of temperature are significant due to the large deformation taking place over a short interval and the relatively low values of heat transfer coefficients making for an almost adiabatic deformation process. None of the trial models provides an accurate response for the thermal behaviour (see Figure 12). This is not too unexpected however since finite similitude does not exist and none of the

thermal parameter were targeted. It is possible of course to capture the thermal behaviour more accurately with matching of thermal physical quantities such as thermal conductivity and specific heat capacity but this would be at the expense of other physical quantities.

Figure 13 presents the contour plot of equivalent plastic strain (EPS) distribution of full and scaled models. It should be noted that with finite similitude, the strain in both full and scaled spaces are identical (i.e. $\underline{\underline{\varepsilon}}_{ts} = \underline{\underline{\varepsilon}}_{ps}$). The same contour intervals is applied to both full and scaled models equivalent plastic strain distributions and the plots are illustrated for the corresponding (synchronised) times, i.e. $t = 0.5ms$, $\tau_{Al} = 0.228ms$ and $\tau_{Tung} = 0.267ms$, where $\tau = t/h$. The spatial variation of the equivalent plastic strain along the radius of the meridian circle for aluminium and tungsten alloy scaled models at different time steps and their replications in the full-scale space are presented in Figure 14 and 15, respectively.

Comparing the results of the Case Studies II and III confirm as expected that by increasing the physical complexity of the problem, the closeness of the replication of the scaled experiment design to the real full-scale design can reduce. The results of two scaled models presented in Figures 10 to 15 indicate that somewhat surprisingly tungsten alloy as the trial material model replicates a more accurate model in the full-scale space for mechanical behaviour.

11. CONCLUSIONS

The presented paper is concerned with a novel methodology in global isotropic scaling of physical phenomena. Based on the developed mathematical theory and the illustrated case studies, following conclusions can be drawn from the presented work:

- The generalised integral form of the conservation laws (i.e. the Euler transport equations) described on synchronised moving control volumes can be used to couple continuum physics between scaled and unscaled spaces.

- The scaling theory can be applied either directly to the physical space or indirectly to the material space and consistent results are obtained in either case.

- The theory although complicated in its development is relatively straightforward to apply and numerical results confirm the applicability of the scaling methodology to thermo-mechanical processes.

- One of the constraints in the practical procedure is finding the optimum trial material model, which is an aspect that warrants further investigation.

Acknowledgements
The authors would like to acknowledge the Higher Committee for Education Development in Iraq and the Department of Electromechanical Engineering at Technology University for providing support for Anees Al-Tamimi to facilitate his doctoral research at the University of Manchester. In addition, acknowledgement and thanks are made to the EPSRC for financial support in the form of an EPSRC HVM Catapult Fellowship to enable Dr Davey to work at the Advanced Forming Research Centre (AFRC) in Glasgow UK.

[1] Barenblatt, G.I., *Scaling*. Vol. 34. 2003: Cambridge University Press.
[2] Yarin, L., *The Pi-Theorem: Applications to fluid mechanics and heat and mass transfer*. Vol. 1. 2012: Springer Science & Business Media.
[3] Buckingham, E., *On physically similar systems; illustrations of the use of dimensional equations.* Physical Review, 1914. 4(4): p. 345.
[4] Sedov, L.I., *Similarity and dimensional methods in mechanics*. 1993: CRC press.
[5] Zohuri, B., *Dimensional analysis and self-similarity methods for engineers and scientists*. 2015: Springer.
[6] Pawelski, O., *Ways and limits of the theory of similarity in application to problems of physics and metal forming.* Journal of Materials Processing Technology, 1992. 34(1-4): p. 19-30.
[7] Kline, S.J., *Similitude and approximation theory*. 2012: Springer Science & Business Media.
[8] Tan, Q.-M., *Dimensional analysis: with case studies in mechanics*. 2011: Springer Science & Business Media.
[9] Ajiboye, J.S., K.-H. Jung, and Y.-T. Im, *Sensitivity study of frictional behavior by dimensional analysis in cold forging.* Journal of mechanical science and technology, 2010. 24(1): p. 115-118.
[10] Abdullah, A., M. Muda, and Z. Samad, *Simulation of Forming Process as an Educational Tool Using Physical Modeling.* International Education Studies, 2008. 1(1): p. 101.
[11] Davey, K. and R. Darvizeh, *Neglected transport equations: extended Rankine–Hugoniot conditions and J-integrals for fracture.* Continuum Mechanics and Thermodynamics, 2016: p. 1-28.
[12] Itskov, M., *Tensor algebra and tensor analysis for engineers*. 2007: Springer.
[13] Darvizeh, R. and K. Davey, *A transport approach for analysis of shock waves in cellular materials.* International Journal of Impact Engineering, 2015. 82: p. 59-73.
[14] von Westenholz, C. *Scale symmetry and virial theorem*. in *Annales de l'IHP Physique théorique*. 1978.
[15] Darvizeh, R. and K. Davey, *Strategies for incorporating material discontinuities into finite element formulations.* Computational Methods For Engineering Science, 2012: p. 167-192.
[16] Johnson, G.R. and W.H. Cook. *A constitutive model and data for metals subjected to large strains, high strain rates and high temperatures*. in *Proceedings of the 7th International Symposium on Ballistics*. 1983. The Hague, The Netherlands.
[17] Simulia, D.S., *Abaqus analysis user's manual.* Dassault Systemes, Pawtucket, USA, 2010.
[18] Meyers, M.A., *Dynamic behavior of materials*. 1994: John Wiley & sons.

Figure(s)

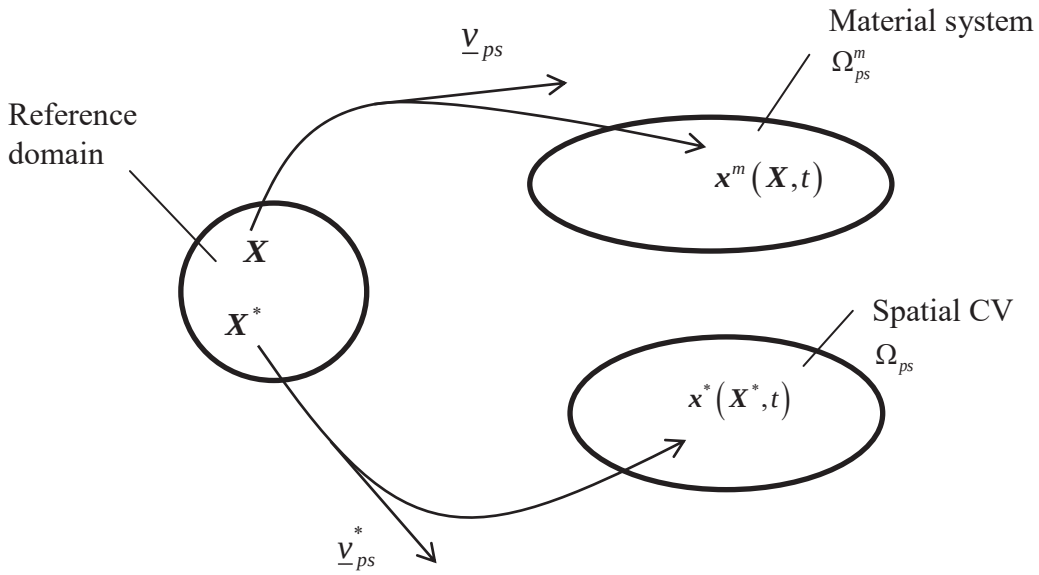

Figure 1. Mapping from reference CV to material system and spatial CV

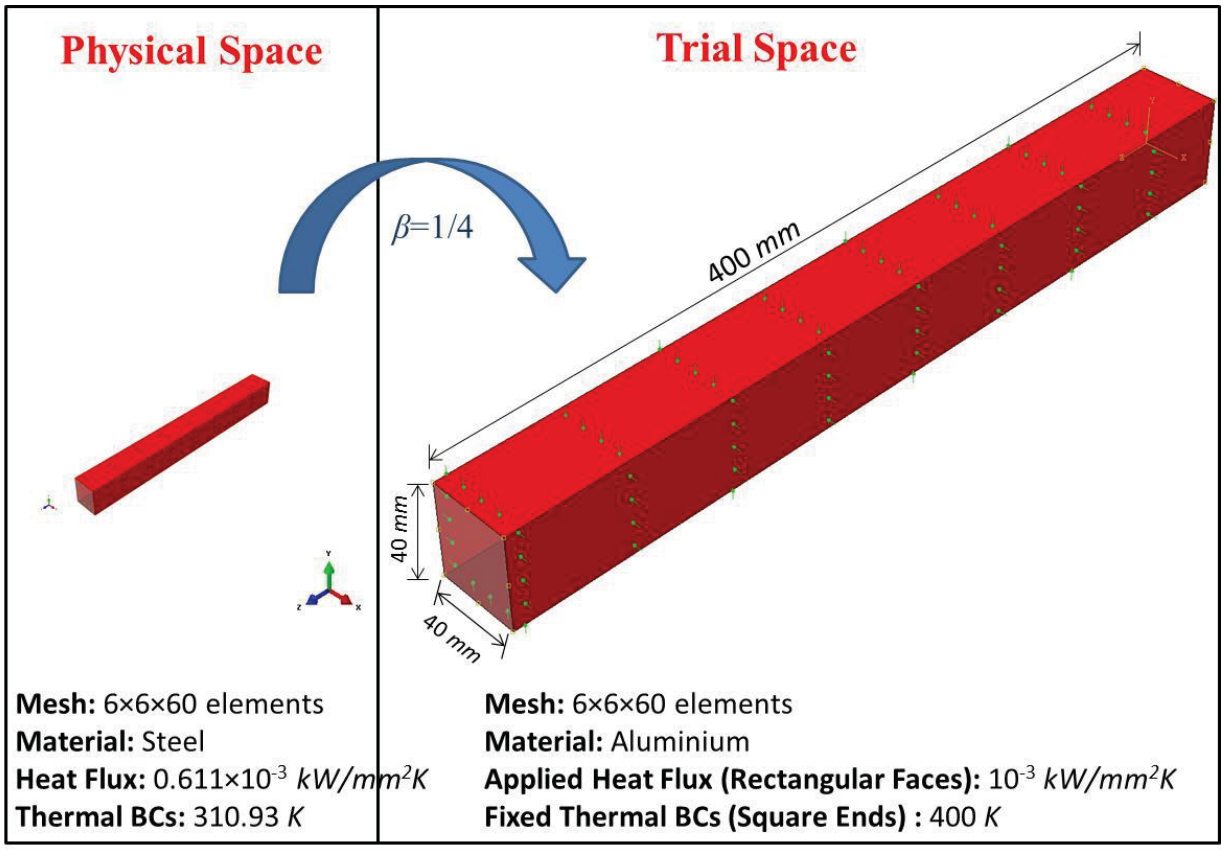

Figure 2. Full and scaled numerical models for Case Study I

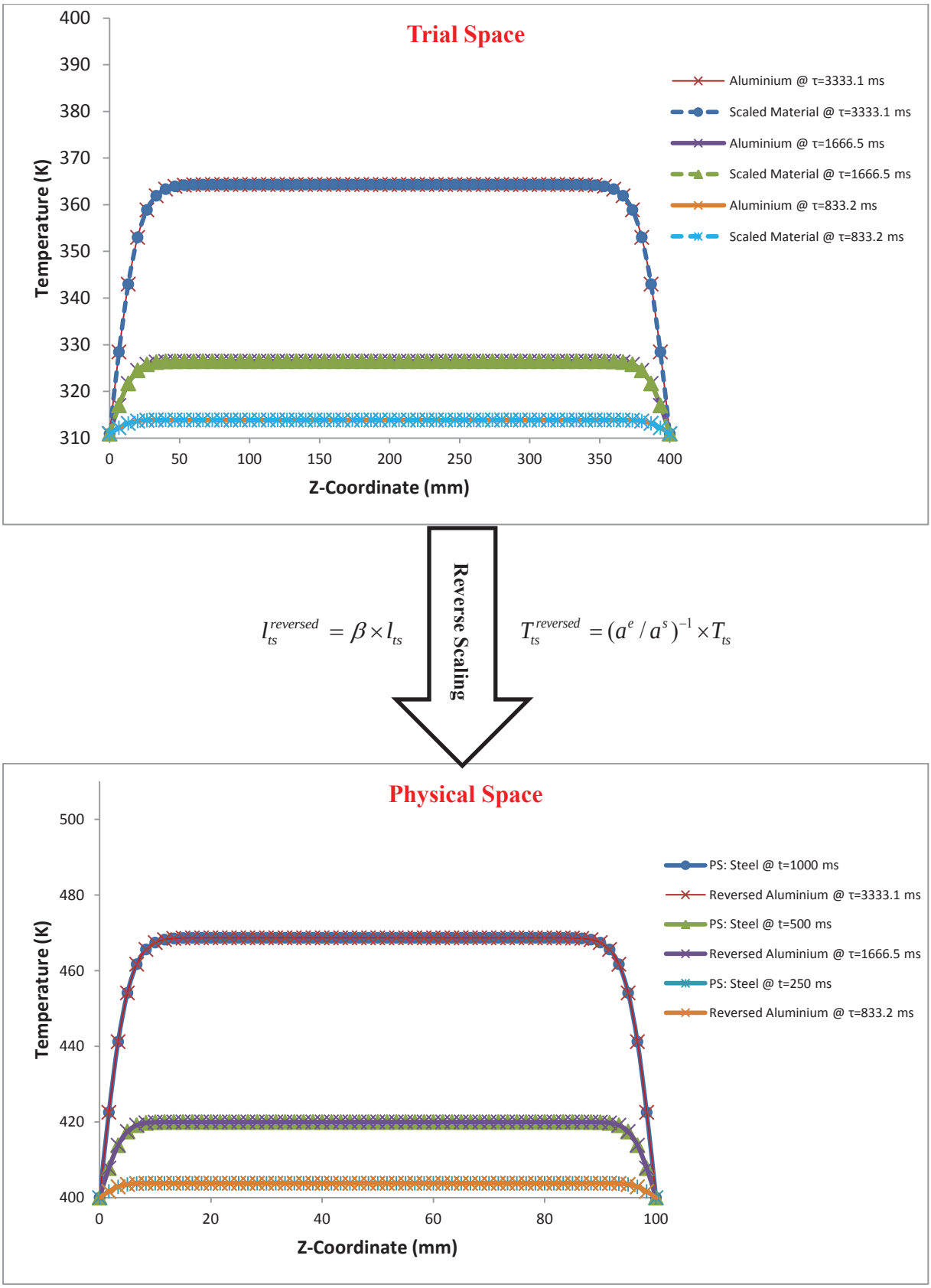

Figure 3. Scaled and full-scale numerical results for the spatial distribution of temperature.

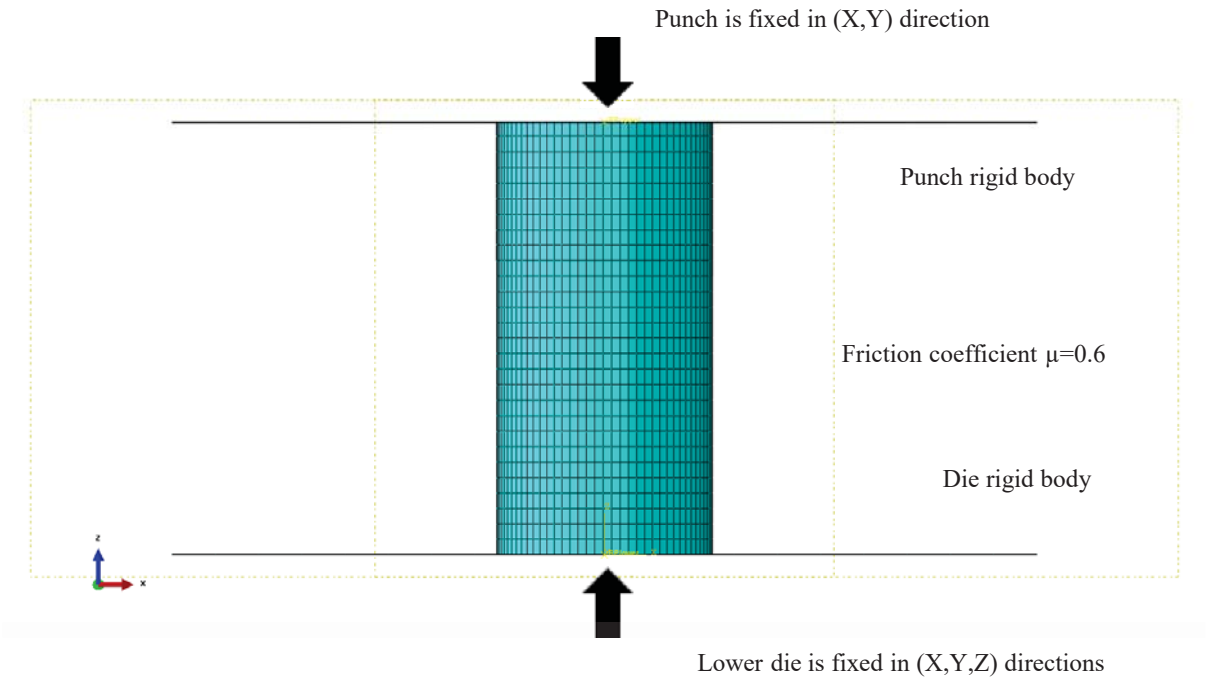

a) Physical Space

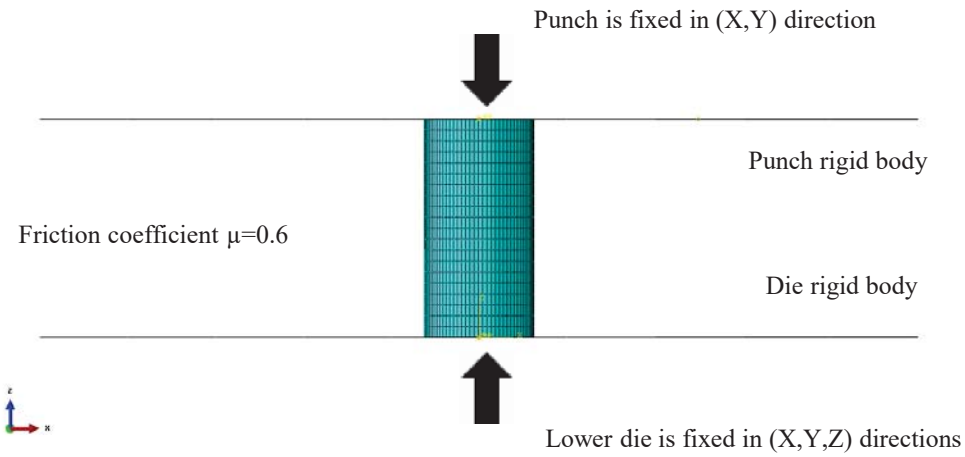

b) Trial Space

Figure 4. Full and scaled numerical models for Case Study II.

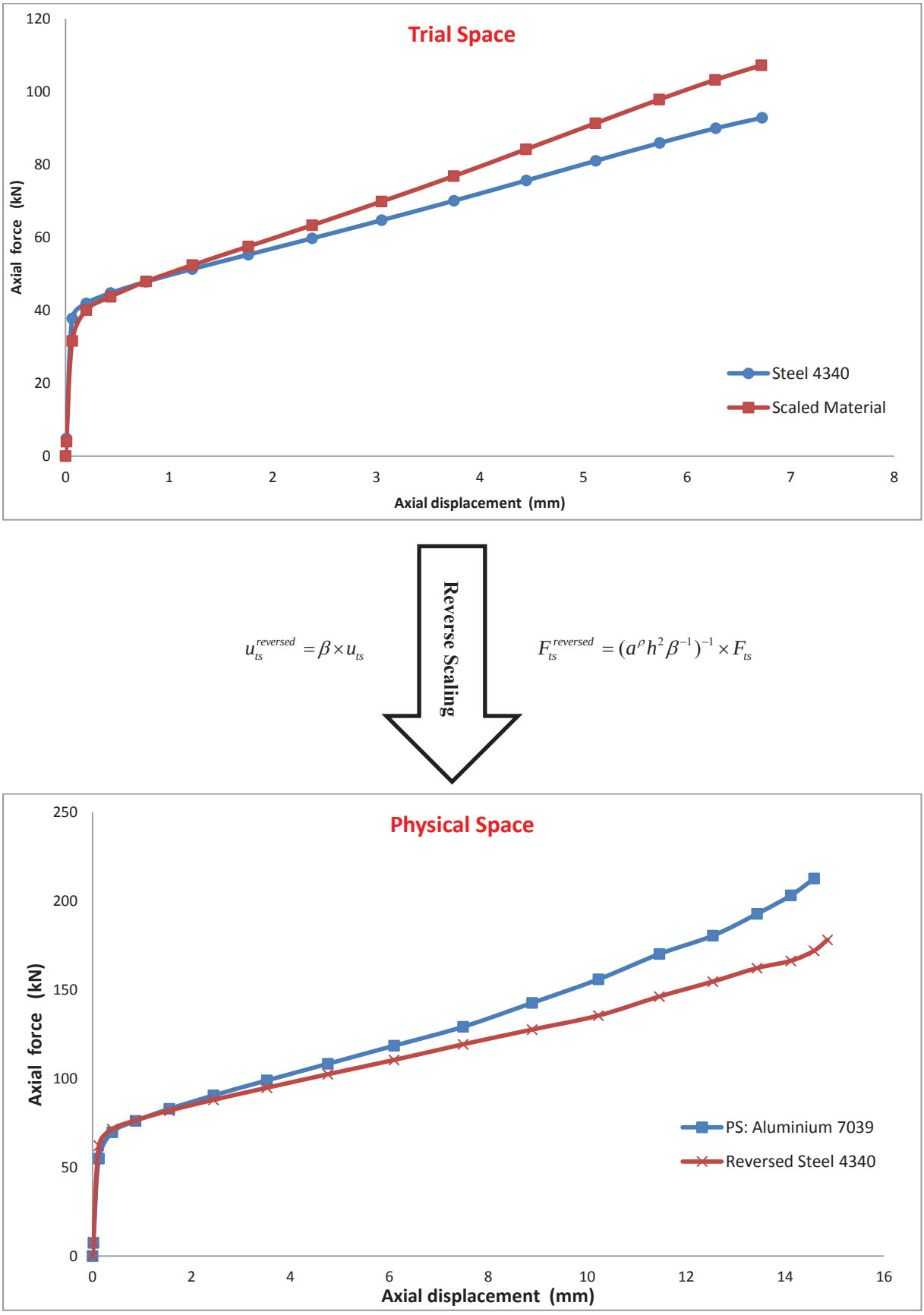

Figure 5. Axial force-displacement results in trial and physical spaces for Design I (trial 1).

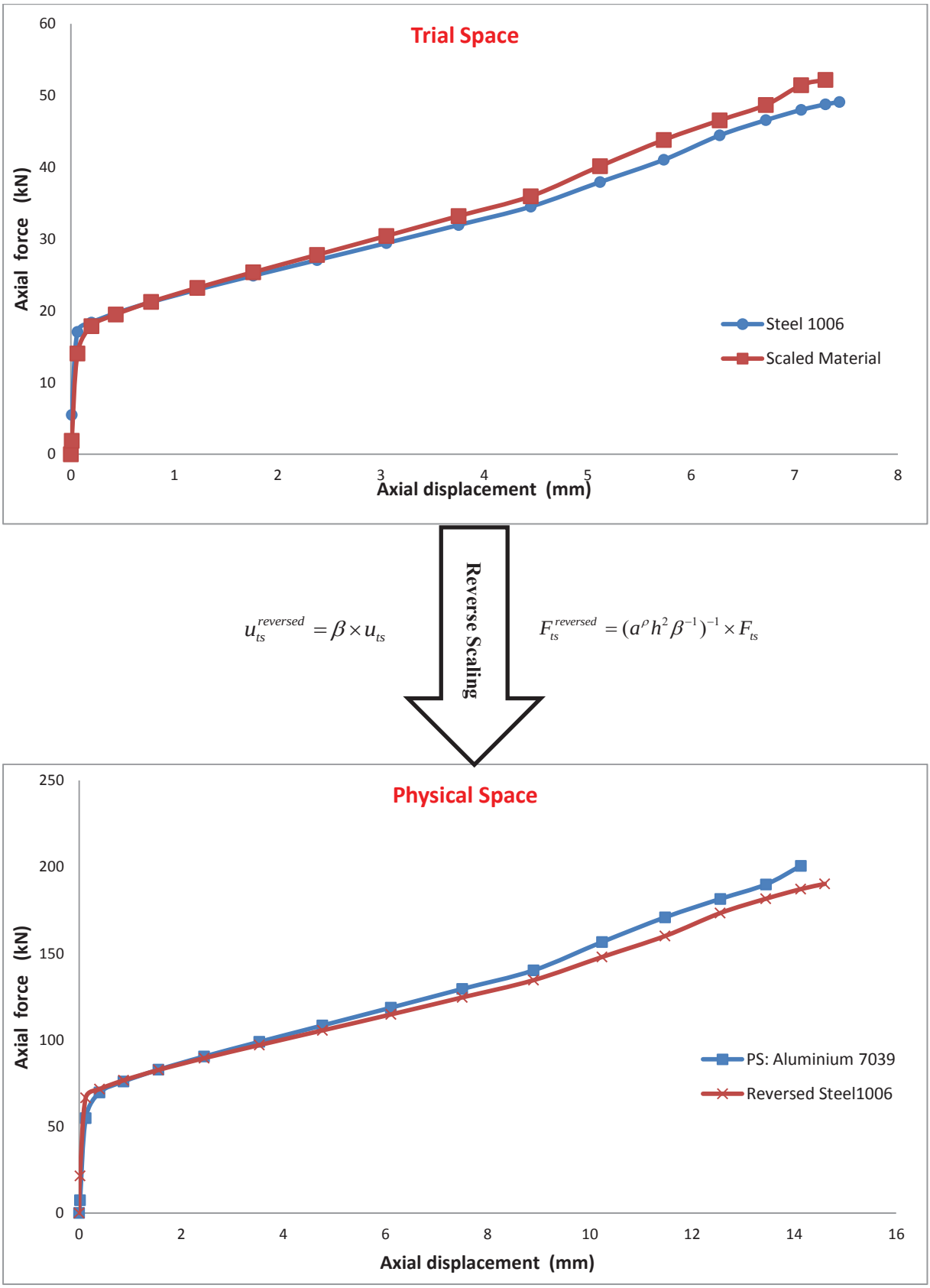

Figure 6. Axial force-displacement curves in trial and physical spaces for Design I (trial 2).

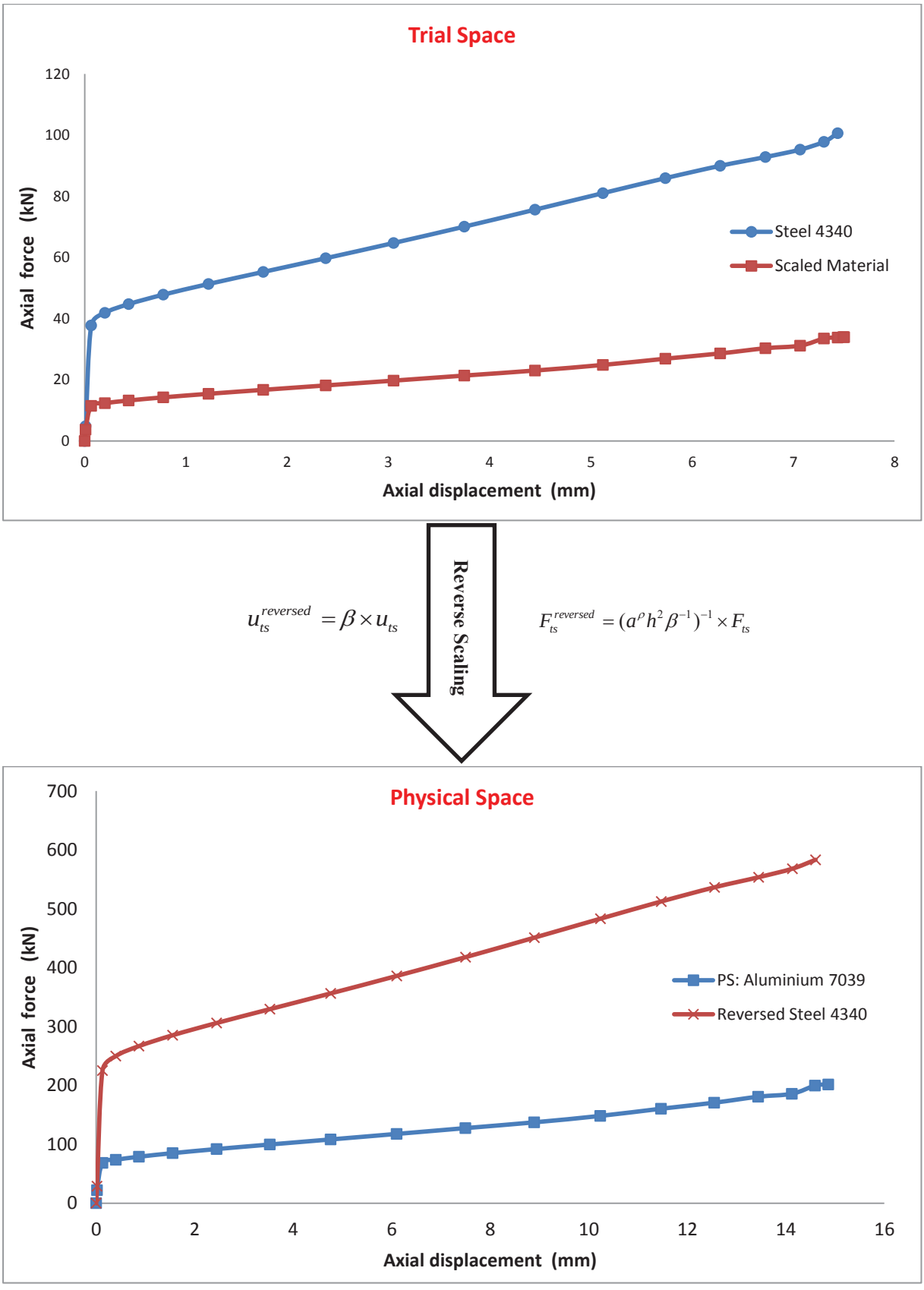

Figure 7. Axial force-displacement curves in trial and physical spaces for Design II (trial 1).

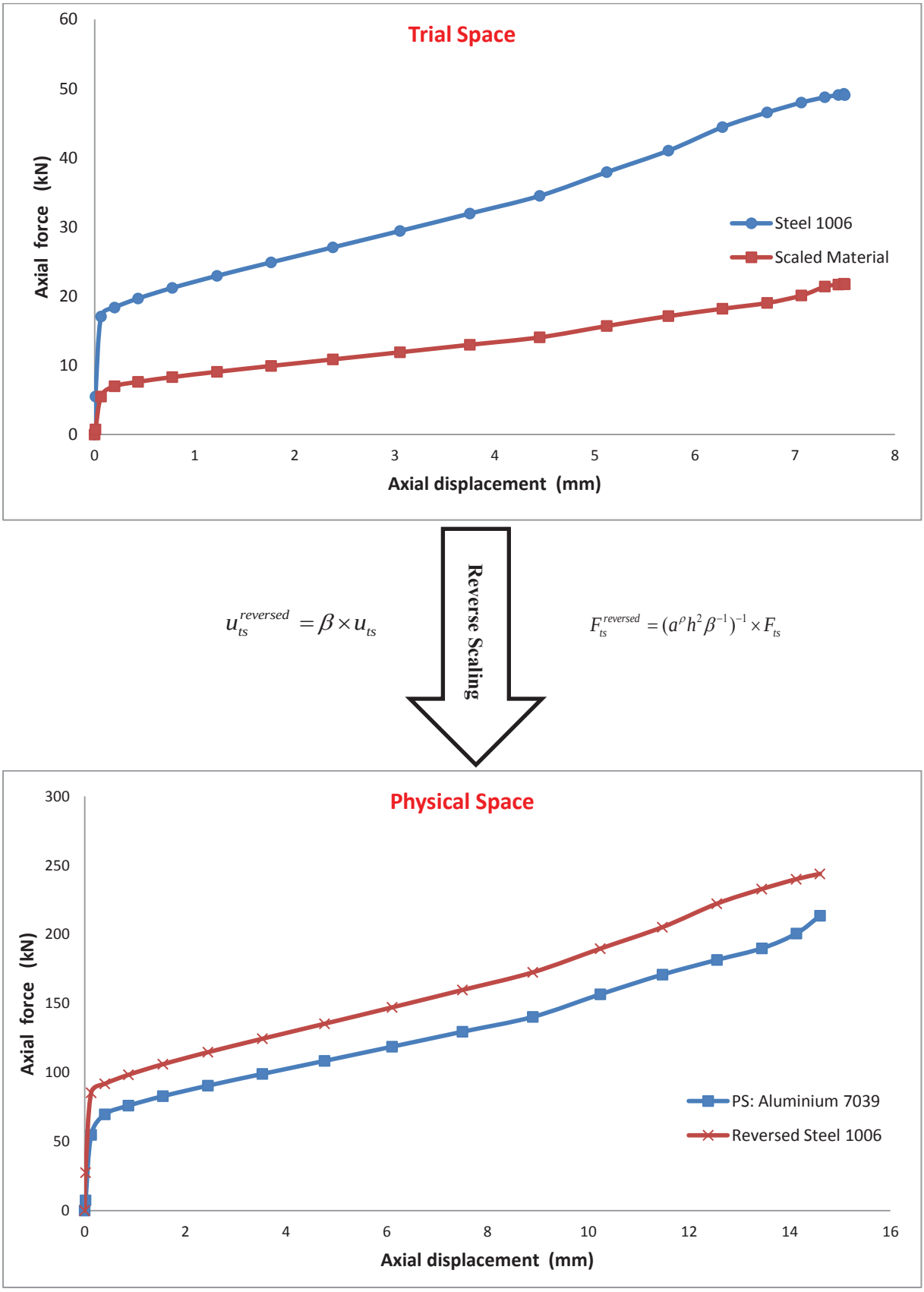

Figure 8. Axial force-displacement curves in trial and physical spaces for Design II (trial 2).

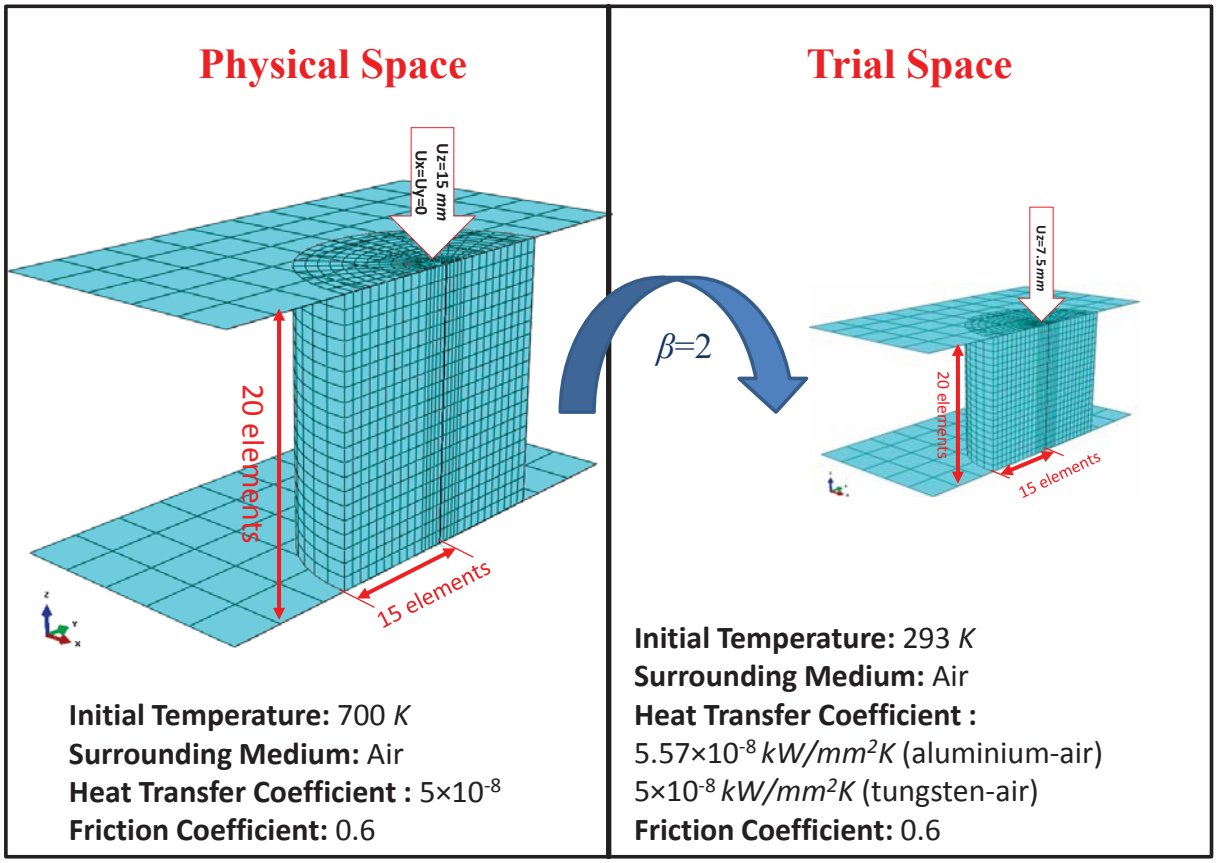

Figure 9. Full and scaled numerical models for Case Study III

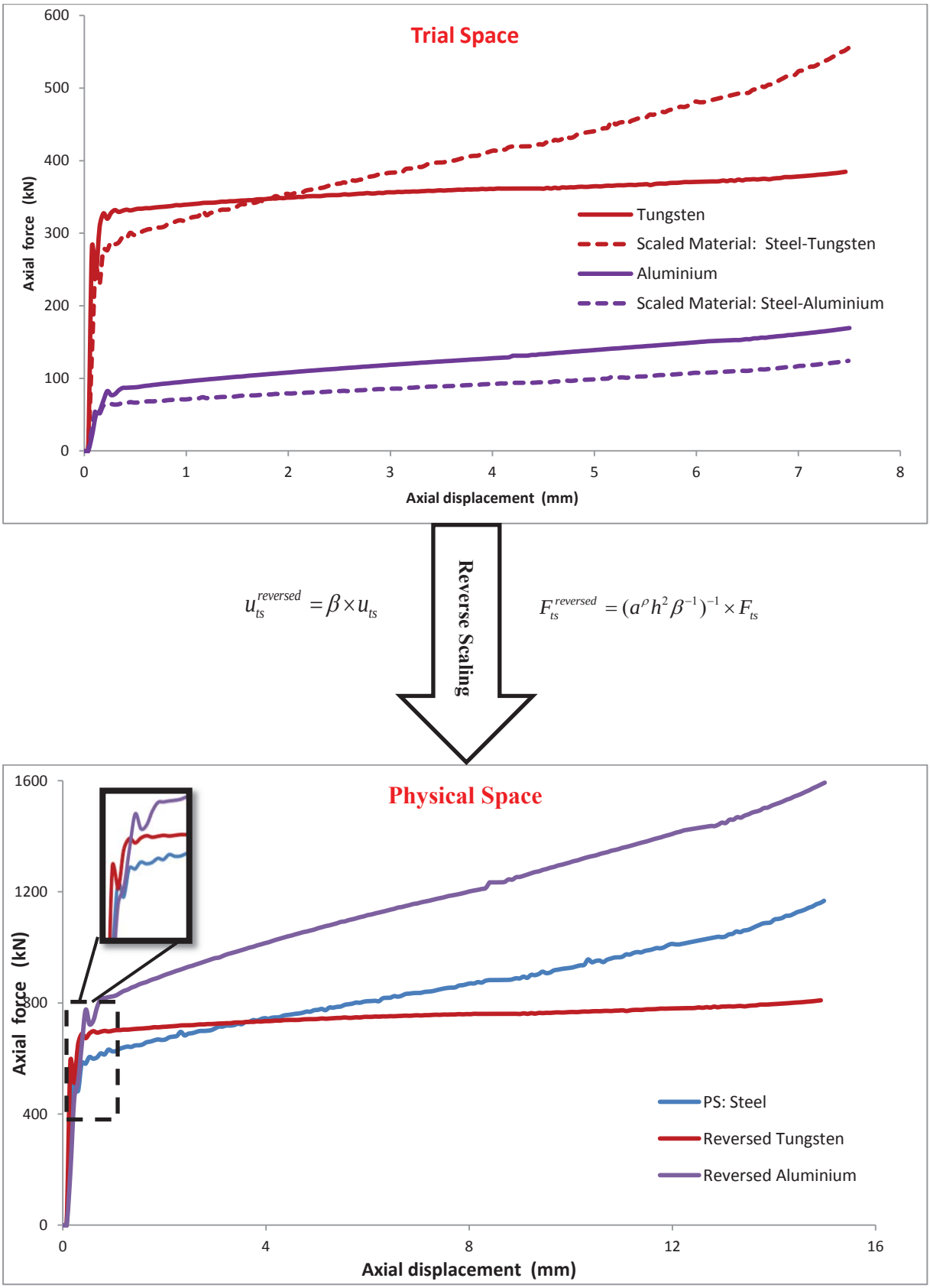

Figure 10. Axial force-displacement curves in trial and physical spaces for case study III.

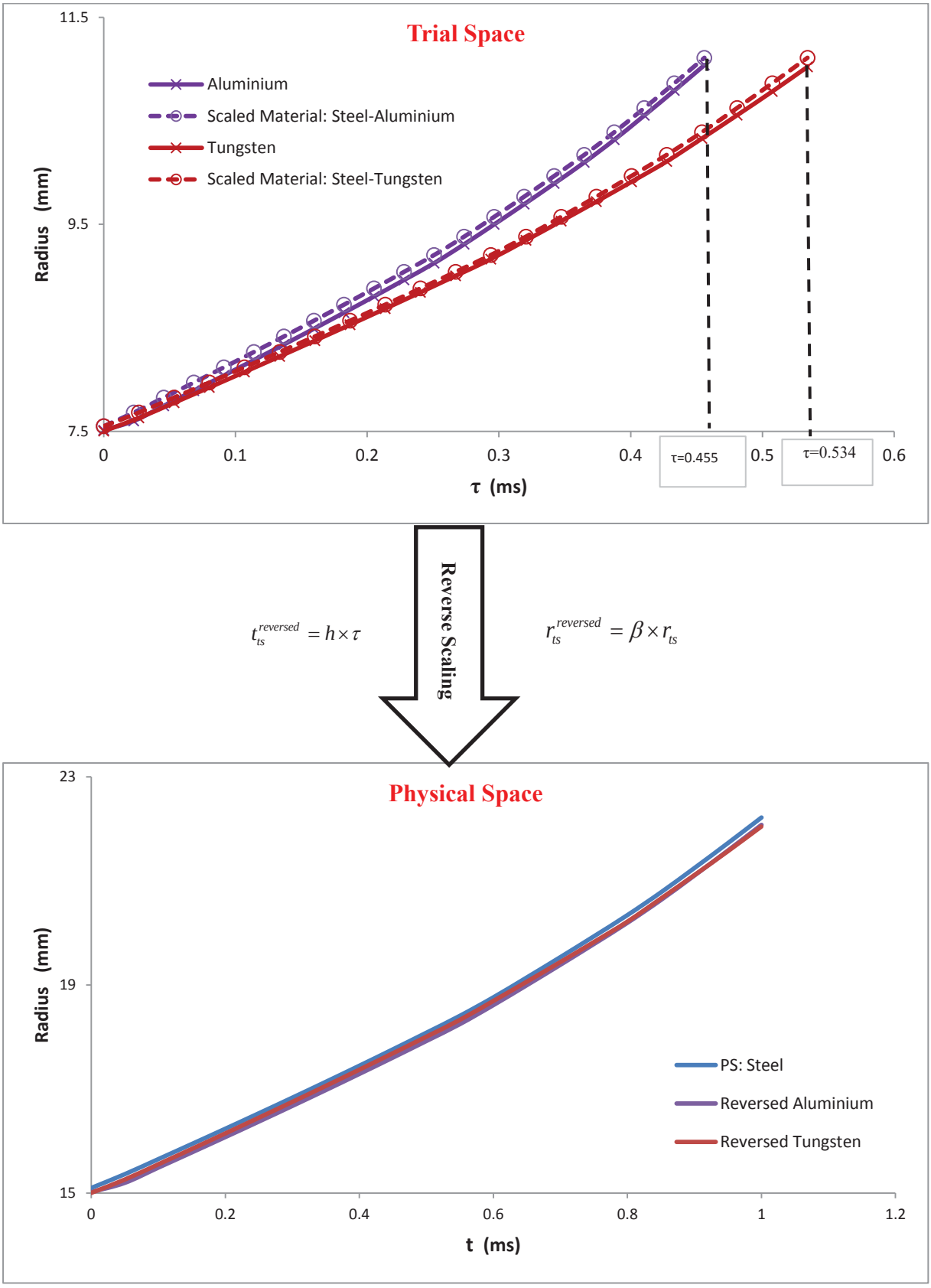

Figure 11. Temporal variation of meridian circle in trial and physical spaces

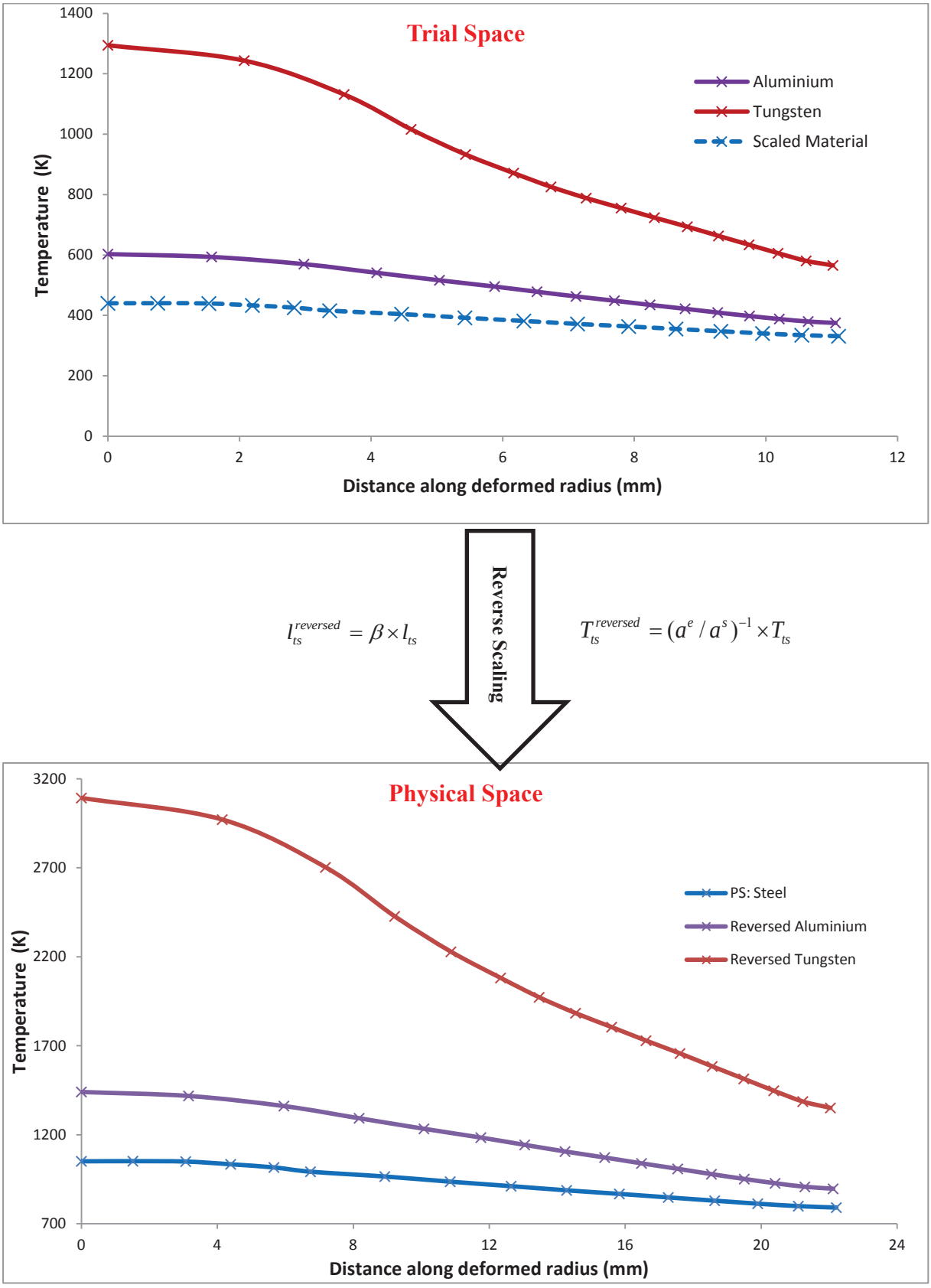

Figure 12. Spatial distribution of temperature in trial and physical spaces at final stages

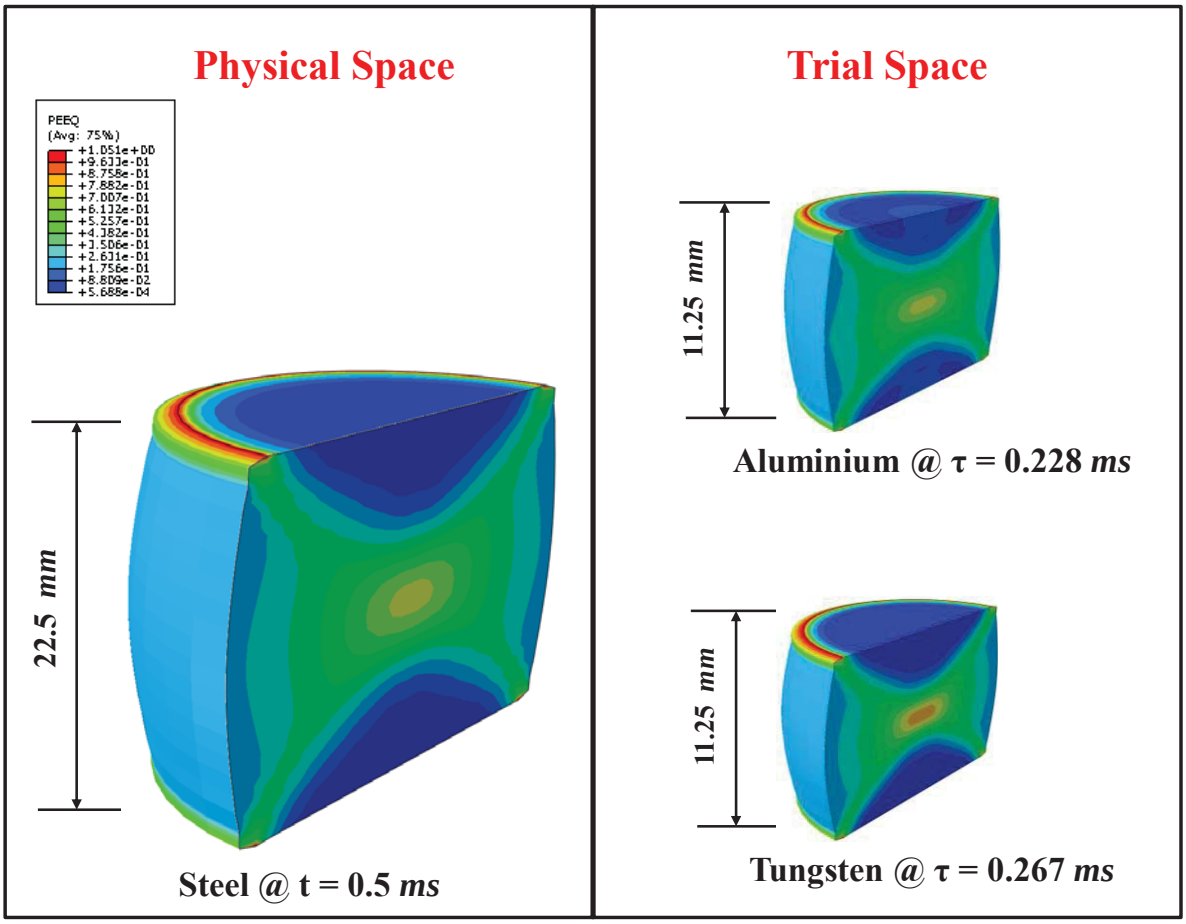

Figure 13. Contour plots of spatial distribution of EPS in physical and trial spaces at specific synchronised times.

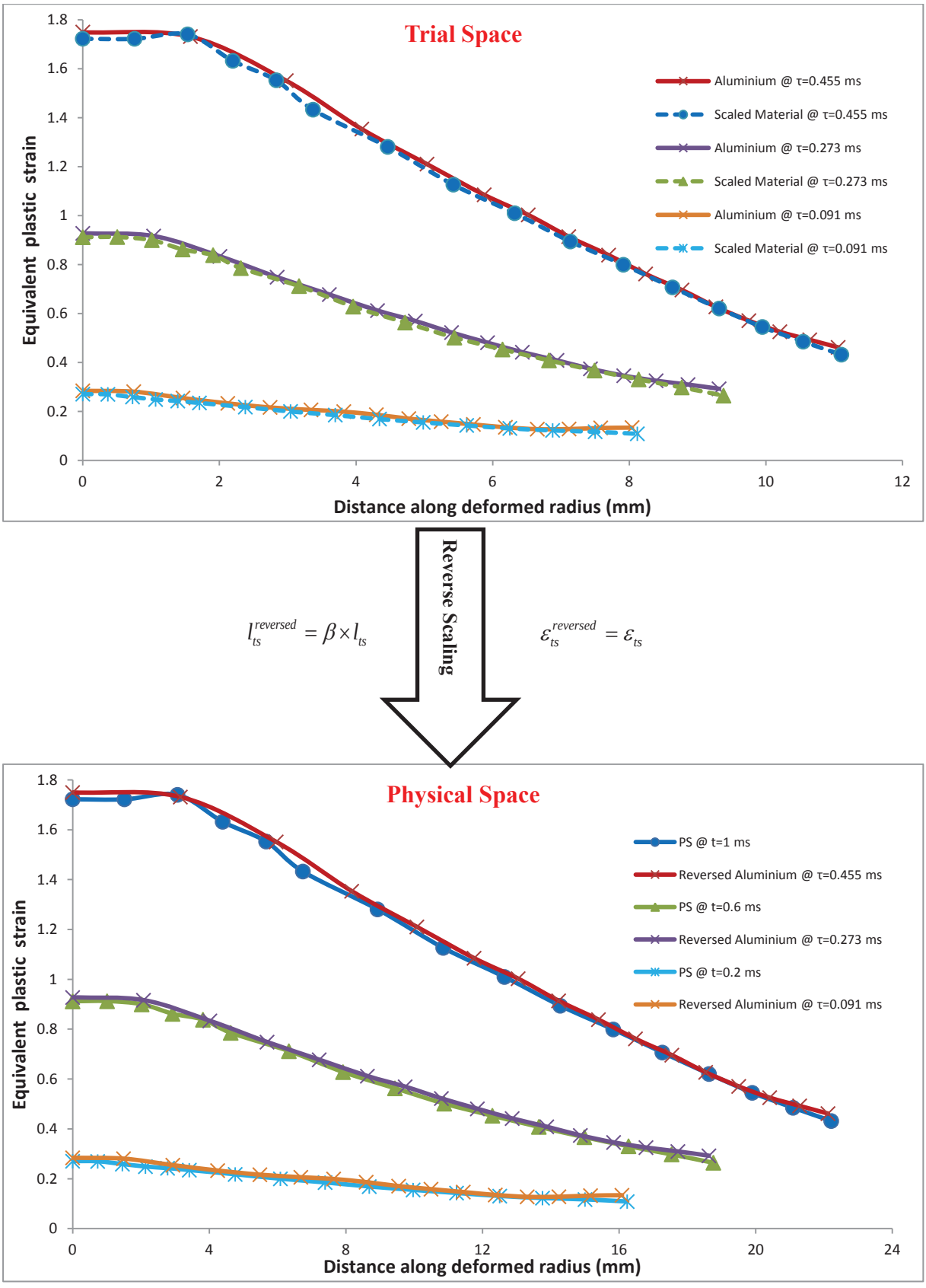

Figure 14. Spatial variation of EPS along meridian circle radius at different times in trial and physical spaces (trial material model: aluminium)

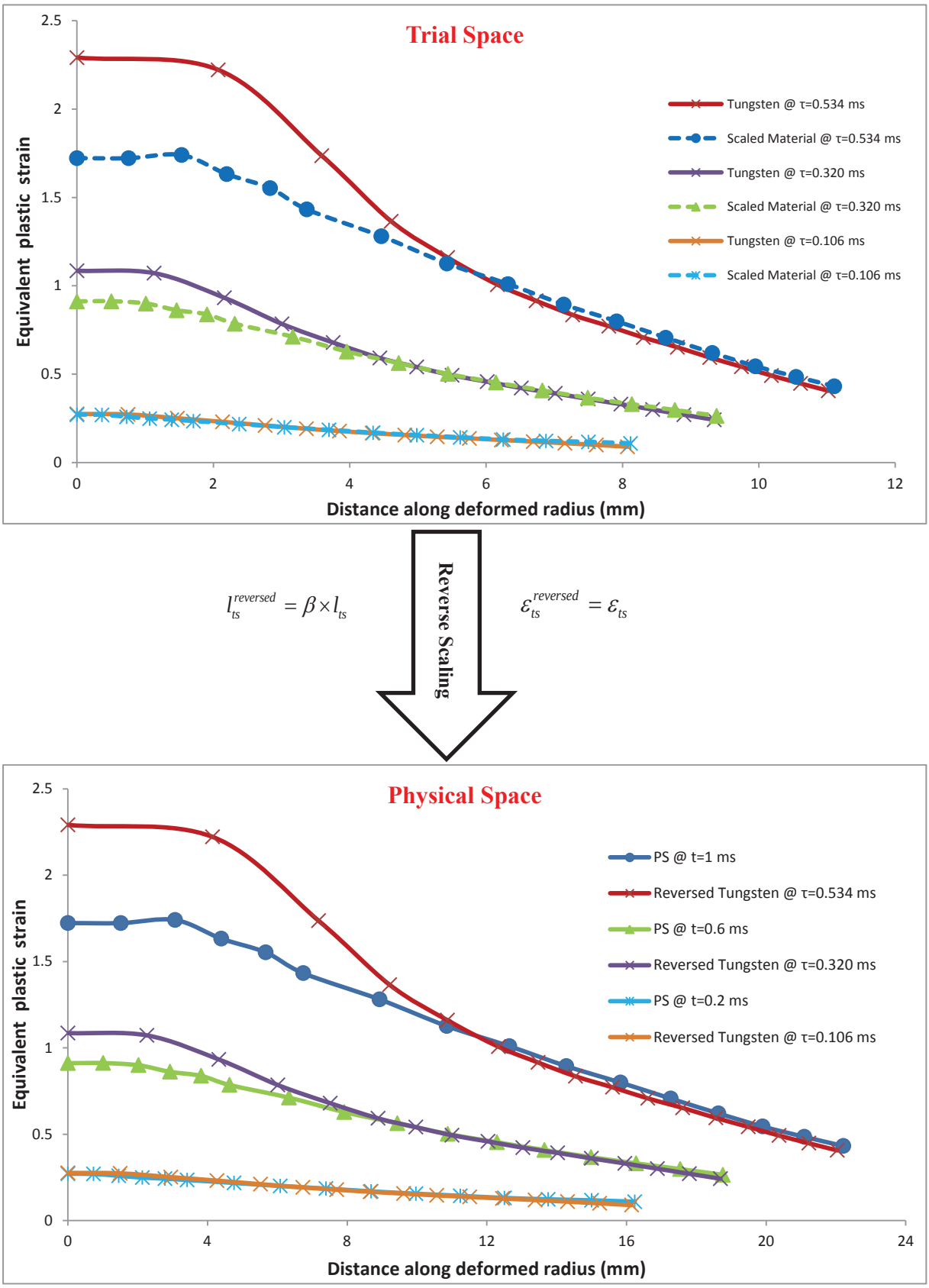

Figure 15. Spatial variation of EPS along meridian circle radius at different times in trial and physical spaces (trial material model: tungsten alloy).